

# **PV Module Troubleshooting and Measurement**

---

**Zihang Ding**

This dissertation is presented for  
Master of Science In Renewable  
Energy of Murdoch University,  
Western Australia

**November, 2012**

Copyright © 2012 Zihang Ding

I declare that this dissertation is my own account  
of my research and contains as its main content work which  
has not been previously submitted for a degree  
at any tertiary institution.

Zihang Ding

## **Abstract**

Over the past few years, the solar photovoltaic (PV) industry has taken the lead in the market growth of the Australian renewable energy industry. Due to the steady manufacturing cost reduction and Australian government support, a great number of PV modules have been installed for domestic and commercial use.

It is well known that the performance of PV modules is greatly influenced by many factors, such as solar irradiance, ambient temperature and the angle of incidence. In addition, the output of PV systems gradually degrades over time under exposure to the sun and other environmental conditions, such as a high temperature and moisture. Normally, the limited warranty period of PV modules ranges from 20 to 25 years, which means the rate of degradation should be less than 1% per year. However, we found that some PV modules performed much worse than the normal ones and their outputs dropped much faster than the expected. Therefore, in any PV module troubleshooting, it is important to figure out the causes that result in dramatic power losses and measure the output of the proper PV modules under operating conditions over a long term.

A rated PV module refers to Standard Test Conditions (STC) of 1000 W/m<sup>2</sup> solar irradiance, Air Mass AM1.5, and a cell or module temperature of 25 °C measured prior to outdoor exposure. However, module performance in real conditions is

variable. Therefore, it is necessary to provide more information on a module in actual operating conditions over a long term.

This study is divided into two parts. The first part is a theoretical analysis of module degradation and troubleshooting techniques. The second part is mainly practical measurements for module degradation estimation. PV module performance measurements are used to obtain highly accurate output data from four different PV modules representing three different technologies: monocrystalline silicon (mc-Si), polycrystalline silicon (p-Si) and laser grooved buried contact crystalline silicon (LGBC, c-Si). Degradation rate estimation is based on comparisons of three groups of previous test results obtained in three different periods (2002, 2003 and 2007) by three PhD Murdoch University students. Finally, a verification process by a simulator is briefly introduced.

## **Acknowledgements**

I really appreciate my major supervisors, Sinisa Djordjevic and Trevor Pryor, for their academic and practical support, and encouragement throughout the project. I also would like to thank Dr. David Parlevliet for providing me with many experimental devices and useful guidance.

## Glossary

<b><u>Abbreviation</u></b>	<b><u>Definition</u></b>
EL	Electroluminescence
IGM	Initial Guaranteed Minimum ( $P_{\max}$ of module)
I <sub>sc</sub>	Short Circuit Current
I <sub>mp</sub>	Maximum Power Current
I-V curve	Current-Voltage Characteristic Curve
LGBC	Laser Grooved Buried Contact
MPP	Maximum Power Point
MPPT	Maximum Power Point Tracker
NREL	National Renewable Energy Laboratory-USA
MU	Murdoch University
mc-Si	Monocrystalline silicon
p-Si	Polycrystalline silicon
$P_{\max}$	Maximum Power
POA	Plant of Array
PL	Photoluminescence
PV	Photovoltaic
STC	Standard Test Conditions-1000W/m <sup>2</sup> , AM Mass 1.5 and 25 °C cell Temperature
TC	Temperature Coefficient
V <sub>mp</sub>	Maximum Power Voltage
V <sub>oc</sub>	Open Circuit Voltage
W	Watt
Wh	Watt.hour
W <sub>p</sub>	Peak Watt
$\eta_c$	Module efficiency
$\kappa$	Temperature Coefficient of Power
$\alpha$	Temperature Coefficient of Current
$\beta$	Temperature Coefficient of Voltage

# Table of Contents

<b>Abstract.....</b>	<b>iv</b>
<b>Acknowledgements .....</b>	<b>vi</b>
<b>Glossary .....</b>	<b>vii</b>
<b>1. Introduction.....</b>	<b>1</b>
1.1 Background .....	1
1.2 Objective of the Thesis .....	2
1.3 Research Focus .....	2
1.4 Thesis Outline .....	3
<b>2. Module degradation.....</b>	<b>4</b>
2.1 Overview of module degradation.....	4
2.2 Cell failure .....	5
2.2.1 Hot spot.....	5
2.2.1.1 Bypass diodes.....	6
2.2.2 Cracks in cells.....	7
2.3 Packaging material degradation.....	8
2.4 Power losses in solar cells.....	9
2.4.1 Fundamental losses .....	9
2.4.2 Recombination.....	10
2.4.3 Series Resistance and Shunt Resistance .....	12
2.4.4 Power loss exceeding the guaranteed level .....	15
2.4.5 Power loss in different strings .....	16
2.5 Module failure.....	18
2.5.1 Dust and Soiling.....	18
2.5.2 Shading .....	19
<b>3. Troubleshooting techniques .....</b>	<b>22</b>
3.1 Visual inspection.....	22
3.2 Infrared imaging (IR).....	22
3.3 Lock in thermography (LIT) .....	23
3.4 Electroluminescence (EL) and Photoluminescence (PL) imaging techniques ..	24
3.5 Resonance ultrasonic vibrations (RUV) technique.....	25
<b>4. PV module performance measurements and degradation rate estimation .....</b>	<b>26</b>
4.1 Background .....	26
4.2 Description of different PV modules used in the project.....	26
4.2.1 Monocrystalline silicon (mc-Si): BP275 & BP585 .....	27
4.2.2 Polycrystalline silicon (p-Si): SX-75 & PW750/70 .....	29
4.3 Major procedures .....	31
4.3.1 Temperature measurement .....	31

4.3.2 Solar Radiation Measurement .....	31
4.3.2.1 <i>Pyranometer</i> .....	32
4.3.3 I-V curve measurement and mapping to STC.....	32
<b>5. Results and discussions.....</b>	<b>34</b>
5.1 STC Test Results .....	39
5.2 Initial STC Test Results .....	39
5.3 STC power after outdoor exposure .....	40
5.4 The rate of module degradation .....	41
<b>6. Limitations and further research .....</b>	<b>43</b>
<b>7. Conclusions and Recommendations.....</b>	<b>44</b>
<b>Reference .....</b>	<b>47</b>
<b>Appendices.....</b>	<b>50</b>
<b>Appendix A</b> Procedure for converting the IV Curve measured in the field to STC using STC Mapping Spreadsheet.....	50
<b>Appendix B</b> Procedures of Prova 210 Solar I-V Tracer .....	58
<b>Appendix C</b> Pyranometers v. Reference Cells for PV Installations .....	59
<b>Appendix D</b> Prova 210 Solar Module Analyzer Accuracy and Reliability .....	61
<b>Appendix E</b> Comparison of I-V curves for different modules under different times of the day.....	62

# **1. Introduction**

## **1.1 Background**

The Photovoltaic (PV) industry has developed very rapidly over the last decade in Australia. Today, more and more PV systems have been installed for both residential and commercial use due to the decreasing price and massive financial support. In 2010, the total installed capacity of PV systems was about 383 MW, which is an increase of 480% over 2009 (Watt et al. 2011). As a result of technological innovation, the efficiency and reliability of PV modules have been greatly improved. However, it is known that some PV modules degrade rapidly and their actual outputs are much lower than normal ones. In addition to power losses, some of modules reveal a number of safety issues caused by cell damage and packaging material degradation. All of the above problems that affect module performance are referred to as module degradation. Normally, the lifecycle of a PV module ranges from 20 to 30 years, which means the rate of module degradation should be less than 1% per year. Nevertheless, it is reported that some modules initially exceed the guaranteed level. Rapid module degradation can lead to short module lifecycle and high replacement cost. Therefore, it is necessary to provide effective troubleshooting techniques and proper module performance measurements for reducing module degradation.

## **1.2 Objective of the Thesis**

The main objective of this project is to investigate the mechanisms of module degradation and compare different troubleshooting techniques. This project also aims to specify the procedure for outdoor measurements of PV module performance and estimate the module degradation rate.

The objectives are achieved by both specific theoretical analysis and practical measurements. The test samples include four different PV modules consisting of three different PV technologies: monocrystalline silicon (mc-Si), polycrystalline silicon (p-Si) and laser grooved buried contact crystalline silicon (LGBC, c-Si).

## **1.3 Research Focus**

The study focuses on the exploration of the mechanisms of module degradation, and module performance measurement and comparison. The fundamental questions that the project will address are:

- How module degradation occurs and how it impacts module performance?
- How to detect module degradation?
- Why comparing results of STC is so important?

## **1.4 Thesis Outline**

This project consists of five components. Firstly, the study discusses the mechanisms and impacts of some typical module degradations. Secondly, some advanced troubleshooting techniques such as infrared imaging (IR) and lock-in thermography (LIT) and electroluminescence (EL) and photoluminescence (RL) imaging are introduced. After that, a series of PV module performance measurements (temperature, solar irradiance, I-V curve characteristics) on four target modules are deployed. The measured results are mapped to STC and compared to three groups of previous results for calculating degradation rate. Anna Carr, who was a Murdoch PhD student, measured the first group of results of the four modules in 2001/2002. Jennifer Martin, who was a MUERI trainee, continued the study over 5 years (2002-2007). Zendegani, another Murdoch MSc student, did further research on the performance for the four modules and obtained the third set of data in 2007. Then, a verification process is used to evaluate the accuracy of the estimated degradation rate. Finally, recommendations and conclusions are presented.

## **2. Module degradation**

### **2.1 Overview of module degradation**

It was not until the early 1970s that information on module degradation was collected (Quintana et al. 2002). However, the work was not well coordinated because the data from various measurement techniques and analytical methods are different and it is difficult to prescribe a standard that makes it easy to compare module degradation. For example, a PV system test demonstrated that module performance lost 1-2% per year during a ten-year period from the mid-eighties to the mid-nineties (Thomas et al. 1994). However, the data from a poly-crystalline module that was continuously exposed outdoors in an open circuit configuration for eight years at Sandia showed that the power loss is around 0.5% per year (King et al. 2000). According to recent research at the National Renewable Energy Laboratory (NREL), it was observed that the performance of both mono- and poly-crystalline, field-aged modules degraded about 0.7% per year, primarily because of short-circuit current losses caused by UV absorption at or near the top of the silicon surface (Osterwald et al. 2002). On the other hand, data from the LEEE-TISO, CH-Testing Centre for Photovoltaic Modules showed that power degradation rates of c-Si modules was between 0.7%-9.8% in the first year and 0.7%-4.9% in the second year (Quintana et al. 2002).

The causes of module degradation are various. Basically, they can be grouped into four categories: cell failure (e.g. cell crack, hot spot), package material degradation

(e.g. delamination, encapsulant degradation, glass breakage), power degradation (e.g. fundamental power losses, recombination, series resistance, etc.), and module failure (e.g. shading, soiling).

## **2.2 Cell failure**

### ***2.2.1 Hot spot***

A hot spot is a very common cell defect that results from cracked or shaded solar cells. Hot spot is characterized by cell overheating induced by short-circuit in series connection (Herrmann et al. 1997). Normally, a PV module consists of several strings, and each string contains more than two series-connected cells. If one of the series-connected cells is shaded or cracked, the operating current produced by the whole string will drop dramatically and approach the short circuit current of the bad cell (Haberlin 2010). In this case, the series connection is short circuited, and the voltage on the bad cell becomes negative and is subjected to the cumulative voltage of all other cells (Haberlin 2010). Such a high reverse biased voltage can result in huge power dissipation in the form of heat. Overheated cells can induce a considerable temperature rise of up to 150°C (Wiesener et al. 1997). The accumulated heat can burn the cells and damage the packaging materials of PV modules. Figure 1 shows some hot spots detected by an infrared camera. In this infrared image, the red colour areas indicate the bad cells which experience the hot spot with a high temperature,

while the light yellow and green areas illustrate the good cells with the normal operating temperature.

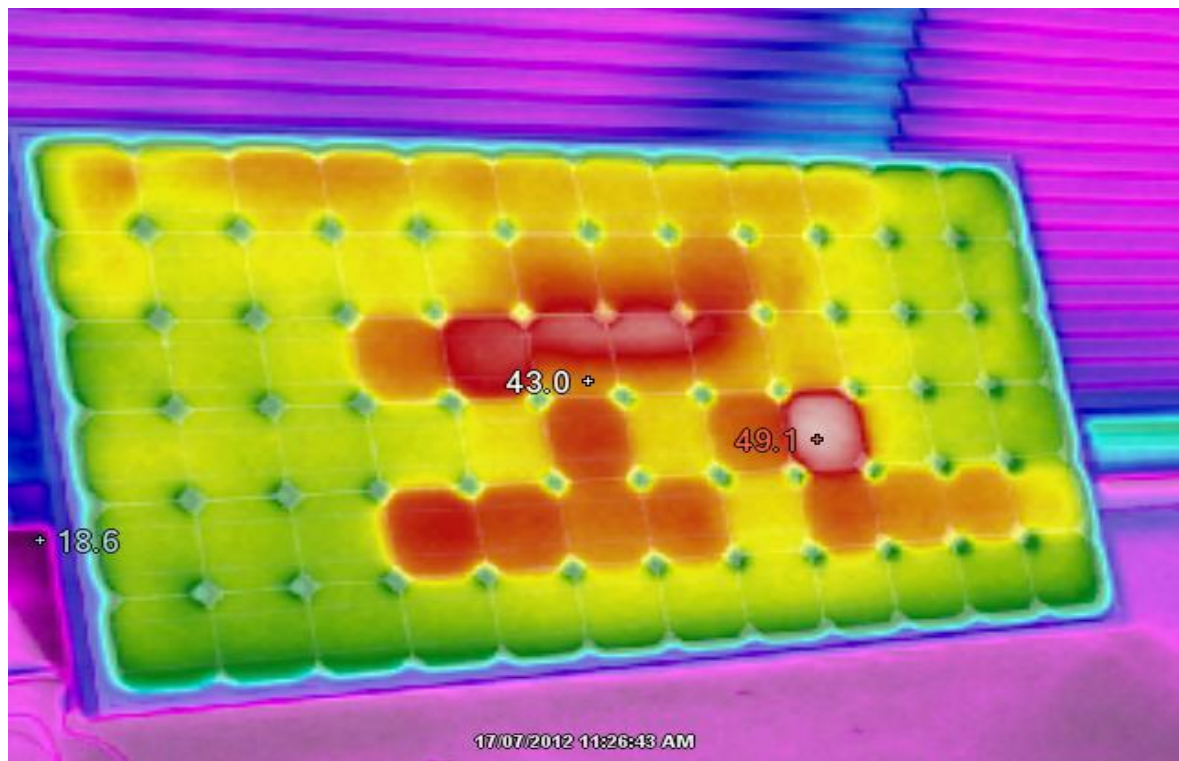


Figure 1: Some hot spot areas detected by an infrared camera

#### *2.2.1.1 Bypass diodes*

Bypass diodes are widely used to minimize hot spot and shading impacts on PV modules. The main procedure is to connect bypass diodes to the shaded string or blocked cells which have a hot spot in parallel. Due to the reverse electrical properties of bypass diodes, the negative voltage induced by a hot spot or shaded cells can lead to a current in the bypass diodes and a short circuit in whole module, which can protect the physical structure (Yanli 2010). Although bypass diodes can extend the lifecycle of PV modules, power losses associated with the current passing through

bypass diodes cannot be avoided (Yanli 2010). If bypass diodes are undersized or suffer failure, they can produce adverse impacts like overheating cells.

### ***2.2.2 Cracks in cells***

A cell crack occurs when solar cells suffer external force or thermal stress. Today, many PV manufacturers try to minimize the thickness of solar cells to reduce the cost. For example, the thickness of a solar cell has decreased from 300  $\mu\text{m}$  to less than 200  $\mu\text{m}$  while the area can be up to 210 mm  $\times$  210 mm (Munoz 2011). This thinner and larger structure makes PV modules more fragile and susceptible to cracking (Munoz 2011). Therefore, cell cracks often occur in manipulation, module lamination and storage. Also, extra thermal stress like hot spot heating can result in cell cracks.

Micro-cracks consist of many tiny cracks that are not often visible by sight but can affect the module performance greatly. Micro-cracks can lead to a loss in cell consistency and trigger recombination problems (Munoz 2011). Sometimes we can see there are different colour lines in the cells even if micro-cracks are not visible. When one uses the electroluminescence (EL) technique to test these coloured lines, there is a good accordance between the lines and micro-cracks (Munoz 2011). By using EL testing, one can see that micro-cracks are darker because there is no light emission or their emission is much lower than other areas. Figure 2 illustrates some micro-cracks are detected by EL imaging technique.

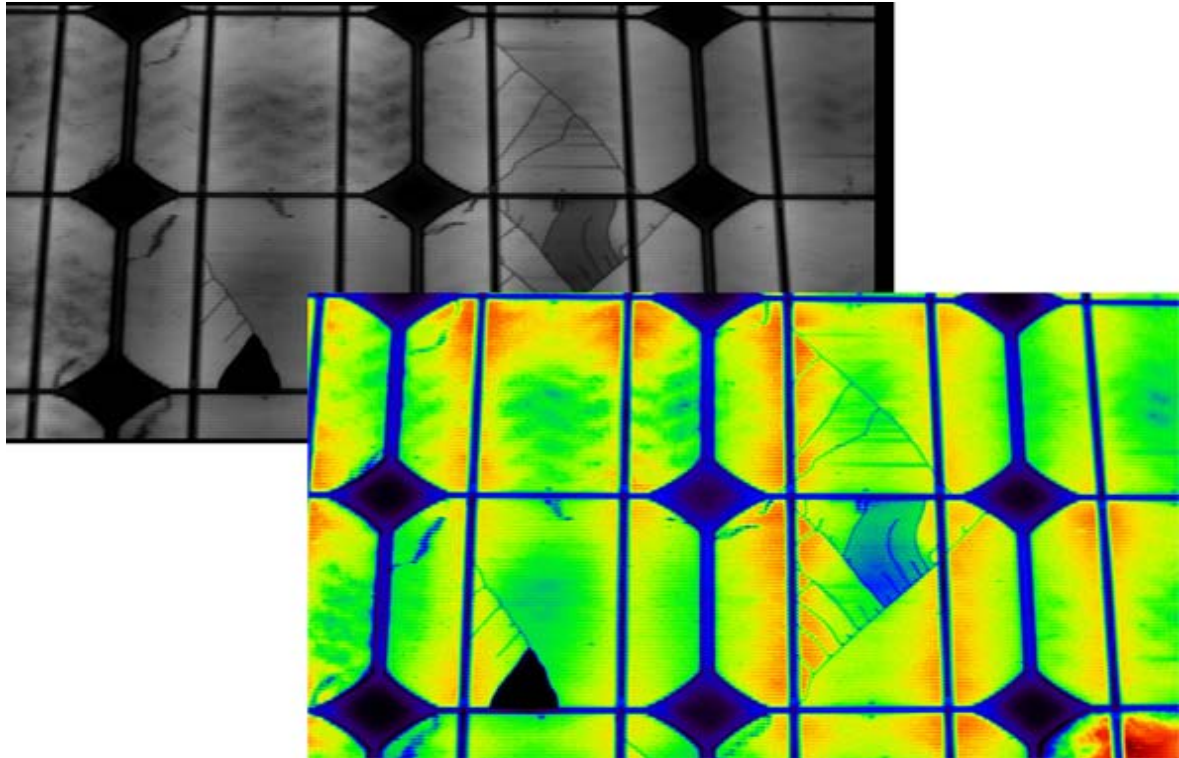


Figure 2: Micro-cracks shown in an EL image (The black and white image is taken by the EL technique; the colour image is taken by an infrared camera)

*Source: (Munoz et al. 2011) "Early degradation of silicon PV modules and guarantee conditions".*

### **2.3 Packaging material degradation**

Module package degradation is a potential issue that can result in poor module performance and a safety hazard. However, it is often overlooked because package degradation is very slow and hard to detect. Although module package material degrades with the aging of the module, hot spot heating, moisture intrusion and wear and tear can accelerate the degradation (Quintana et al. 2002). Some typical module package degradations include glass breakage, encapsulant discoloration and delamination.

Package damage can result in excessive leakage current and ground faults (Quintana et al. 2002). In addition, package damage can produce safety hazards in high voltage systems due to the lack of protective insulation. Such failures may induce electric shock and create a pathway for electrochemical corrosion (Quintana et al. 2002). The potential shock hazard can be worsened by moisture intrusion into the package.

## **2.4 Power losses in solar cells**

### ***2.4.1 Fundamental losses***

Photovoltaic energy conversion relies on the quantum nature of light, which it is seen as a flux of particles, called photons, which carry the energy (Markvart 2000). Equation (1) demonstrates that each photon carries the energy. However, only a part of photons can be converted into electricity by solar cells. On a clear day, about  $4.4 \times 10^{17}$  photons on average reach a square centimeter of the Earth's surface every second (Markvart 2000). However, not all the photovoltaic energy can be absorbed and transformed to electricity by the solar cells because only those photons whose energy in excess of the band-gap are available. Solar cells are made from semiconductors, so when such a photon goes into solar cells, the absorption process produces electron-hole pairs.

$$E_{ph}(\lambda) = \frac{hc}{\lambda} \quad (1)$$

Where  $h$  is the Planck constant,  $c$  is the speed of light, and  $\lambda$  is the wavelength of light.

The nature of the absorption process also proves that there is a fraction of power from photons lost in the form of heat (See Figure 3). It is because all the generated electron-hole pairs have energy in excess of the band-gap; however, their states will decay to near the edges of their respective bands immediately (Markvart 2000). Also, the second law of thermodynamics proves that there is a conversion efficiency limit for a solar cell therefore the fundamental power losses cannot be avoided.

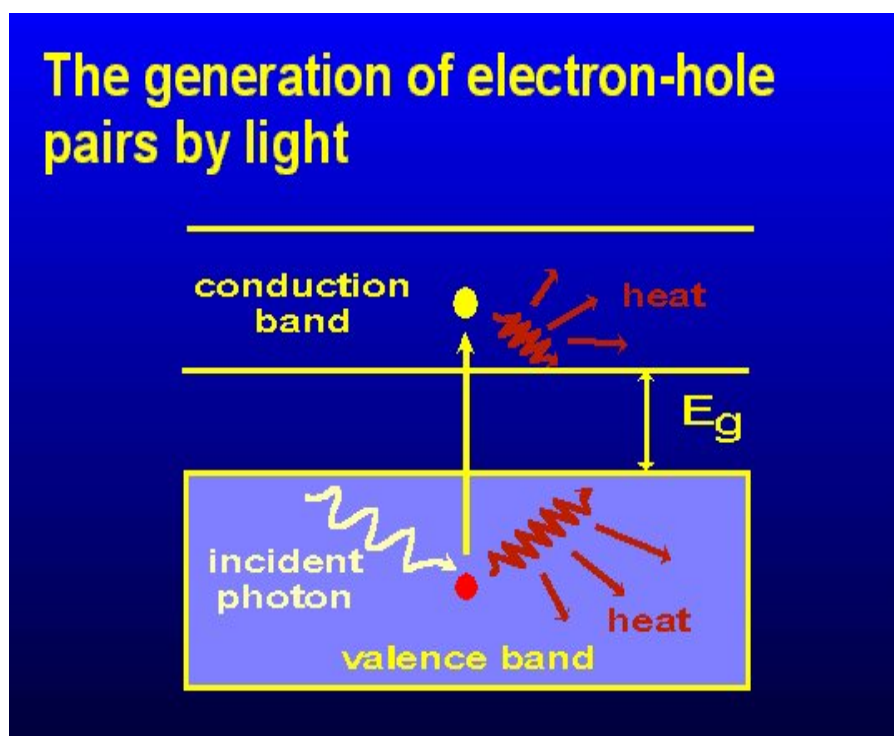


Figure 3: The generation of electron-hole pairs by light

Source: (Markvart 2000) "Solar Electricity"

### 2.4.2 Recombination

Recombination is defined as an opposite process to carrier generation when an electron-hole pair disappears (Markvart 2000). Recombination occurs when the electrons fall back into the valence band and recombine with holes. In this case, both

the voltage and current will be reduced and therefore the power output decreases. (Markvart 2000).

Surface recombination and recombination at contacts are two common types of recombination. As shown in Figure 4, there are two ways for minimizing the recombination losses: one is to attach a layer of passivating oxide to reduce surface recombination; the other is to surround the contacts by heavily doped regions acting as “minority-carrier mirrors” which can prevent the minority carriers from getting into the contacts and recombining (Markvart 2000).

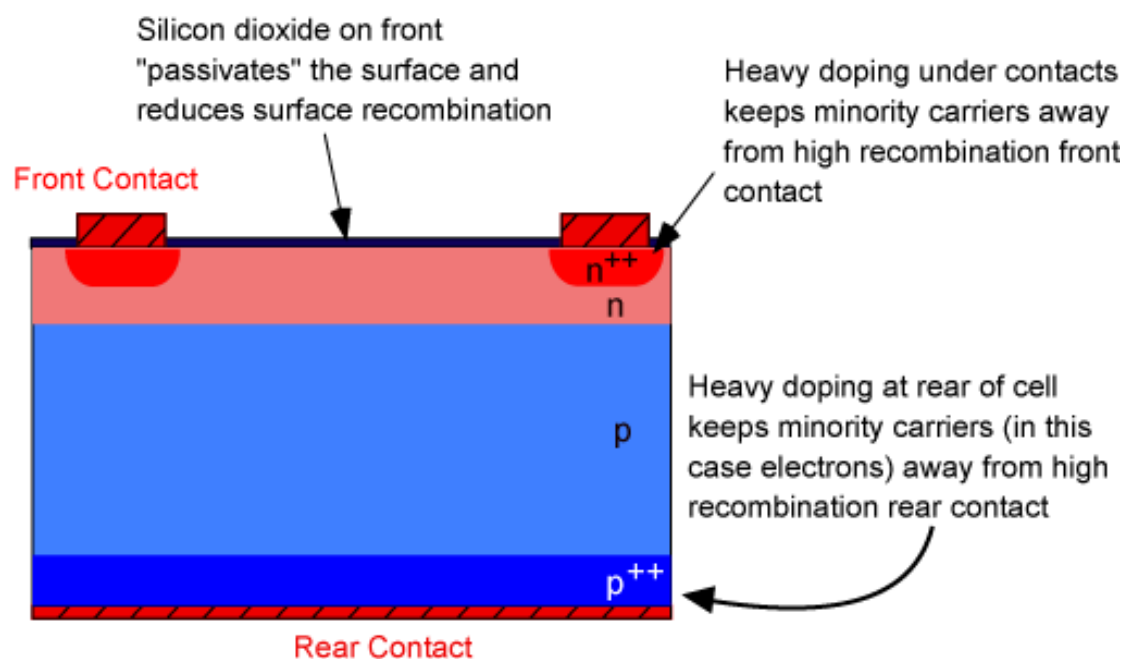


Figure 4: Silicon dioxide layer and heavy doping at rear of cells for reducing surface recombination and recombination at contacts

Source: <http://pveducation.org/pvcdrom/design/surface-recombination>

### 2.4.3 Series Resistance and Shunt Resistance

Both series resistance ( $R_S$ ) and shunt resistance ( $R_{SH}$ ) can impact PV module performance. As the equivalent circuit of a solar cell (Figure 5) shows, increasing  $R_S$  can lead to a drop in  $I_{sc}$ , while decreasing  $R_{SH}$  can result in  $V_{oc}$  reduction.

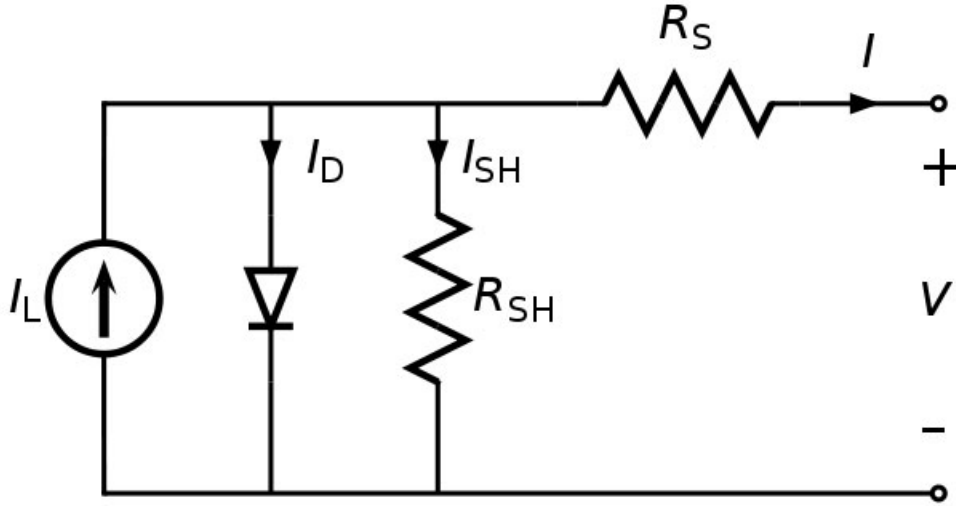


Figure 5: An equivalent circuit of solar cells

Source: (Emery 2011). *Handbook of Photovoltaic Science and Engineering*

The fill factor (FF) is defined as the ratio of the maximum power point (MPP) to  $I_{sc}$  times open-circuit voltage  $V_{oc}$  (See Equation 2). Figure 6 and Figure 7 illustrate the effects of  $R_S$  and  $R_{SH}$  on the  $I$ - $V$  characteristics of solar cells. It can be seen that both FF and MPP reduce as  $R_S$  increases and  $R_{SH}$  decreases.

$$FF = \frac{I_{mp} \times V_{mp}}{I_{sc} \times V_{oc}} \quad (2)$$

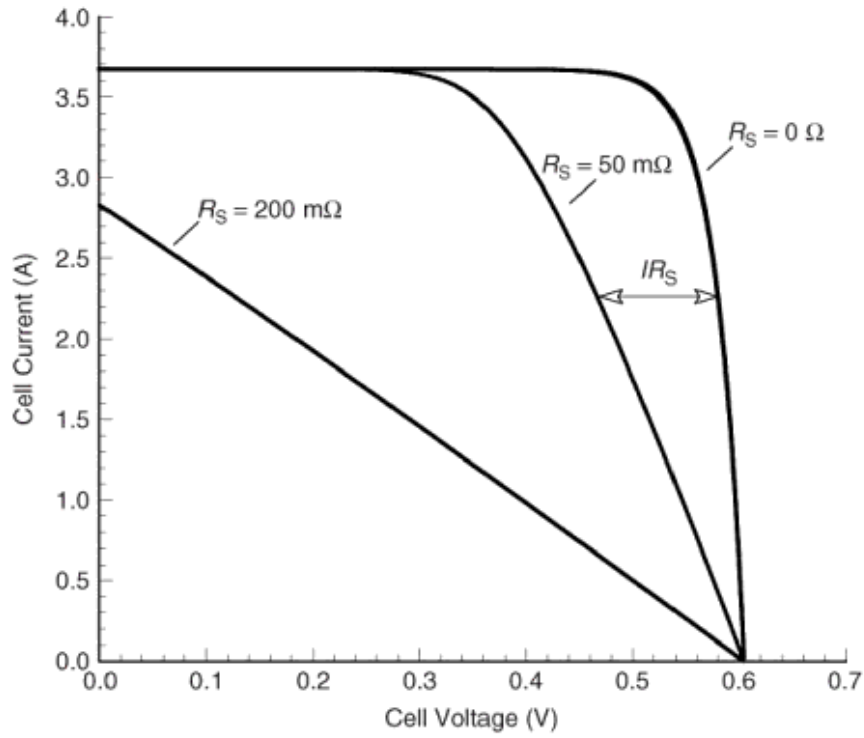


Figure 6: Effect of series resistance on the  $I$ - $V$  curves of solar cells  
Source: (Emery 2011). *Handbook of Photovoltaic Science and Engineering*

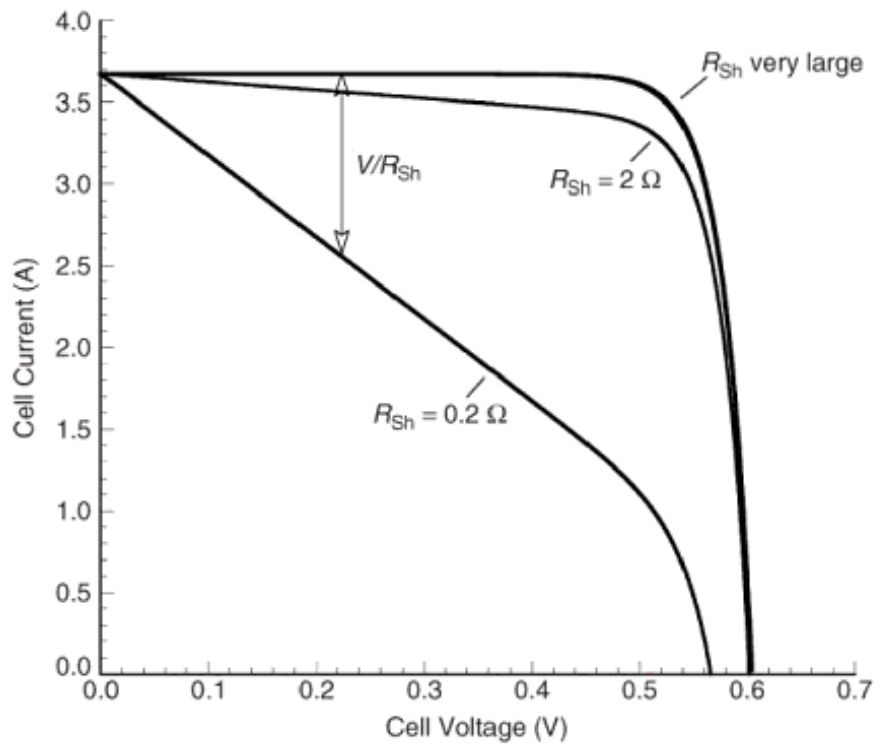


Figure 7: Effect of shunt resistance on the  $I$ - $V$  curve of solar cells  
Source: (Emery 2011) *Handbook of Photovoltaic Science and Engineering*

Normally,  $R_S$  increase results from delamination of contacts or corrosion induced by water vapor while  $R_{SH}$  decrease is mainly due to hot spot, partial shading, thermal stress and localized ohmic shorts (Alers et al. 2011). Figure 8 shows the simulation results for a given module with one cell shaded 50% and a range of shunt resistances for the cell. It can be found that a shaded cell leads to  $R_{SH}$  decrease and MPP reduction, while an unshaded cell has no impact. The thermal stress results from the module temperature increase can cause  $R_{SH}$  decrease. Figure 9 illustrates a log-normal distribution of the shunt resistance in an unstressed module and a stressed module. It is seen that the distribution of  $R_{SH}$  of the stressed module becomes broader and shifts to a smaller value (Alers et al. 2011).

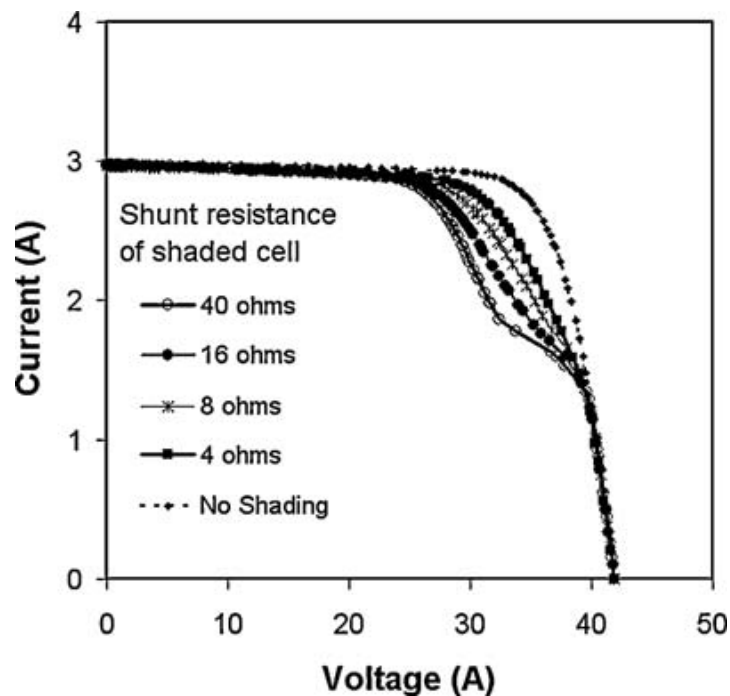


Figure 8: Simulation results for the module with one cell shaded 50% and a range of shunt resistances for the cell

Source: (Alers et al. 2010) "Degradation of individual cells in a module measured with differential IV analysis"

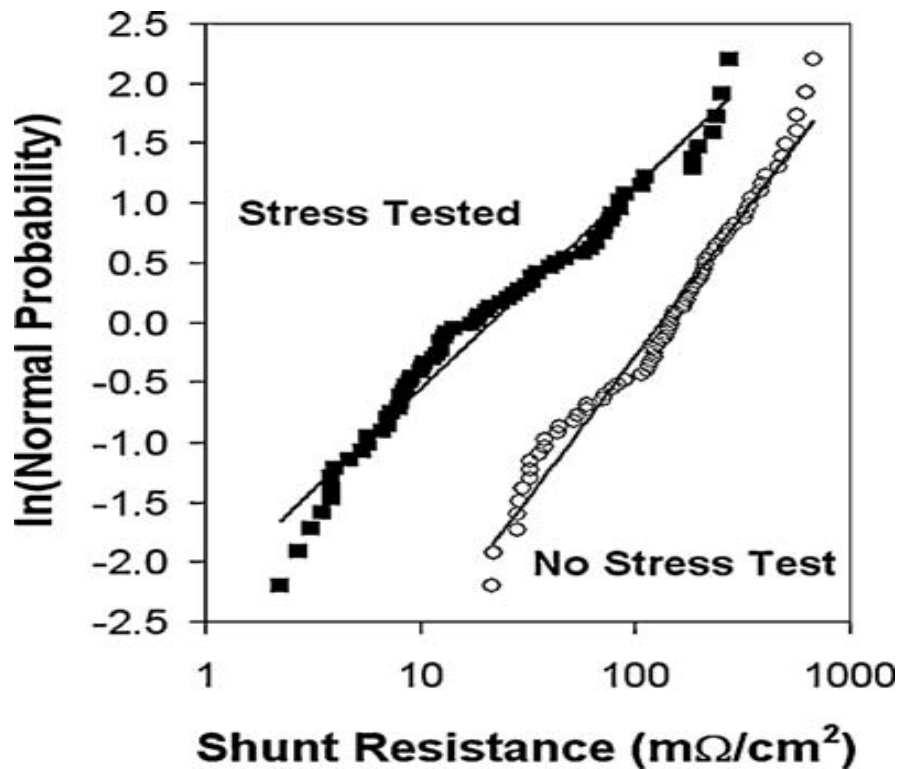


Figure 9: Log-normal distribution of the shunt resistance in an unstressed module and a stressed module

Source: (Alers et al. 2010) “Degradation of individual cells in a module measured with differential IV analysis”

#### **2.4.4 Power loss exceeding the guaranteed level**

Every module has its own rated maximum power and the allowed tolerance, and this information can be obtained under standard test conditions. Also, manufacturers regulate the guaranteed power that a module can deliver. Normally, the guaranteed power is 90% of the rated maximum power for a period of 10-15 years (Munoz 2011). If the time is increased up to 20-25 years, the guaranteed power will decrease to 80% of the rated maximum power. However, some new modules have been found to have higher power losses than their guaranteed level after only a few weeks (Munoz 2011). Measuring the representative samples periodically can detect significant power loss

higher than the guaranteed level but it is difficult because all the samples must be disconnected from the solar plant when they are under examination (Munoz 2011).

#### 2.4.5 Power loss in different strings

As shown in Figure 10, there is a problem occurring in one string of cells due to a jump in the  $I$ - $V$  curve. The  $I$ - $V$  curve analysis can be used to measure module performance string by string. By comparing different  $I$ - $V$  curves from different strings, the defective areas can be detected. Figures 11-13 represent the  $I$ - $V$  curves of the three strings of 24 cells in a module. The  $I$ - $V$  curves not only show the current and voltage changes but also indicate the maximum power point (the blue dot). The current in the central string of cells is much lower than the other strings, this indicates a defect in this area. The right side string is not normal and has defects while the left side string looks good.

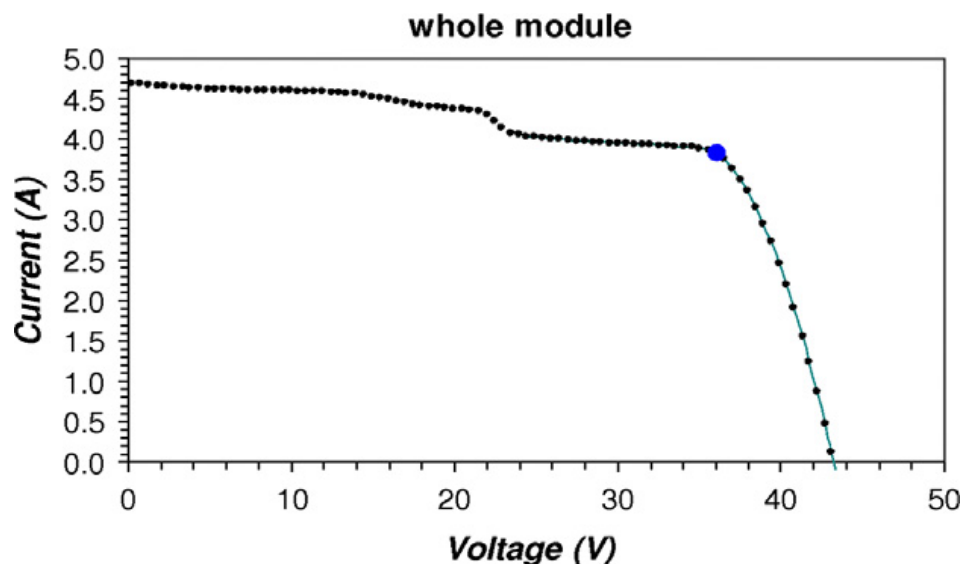


Figure 10: Electrical  $I$ - $V$  curve of a defective module

Source: (Munoz et al. 2011) "Early degradation of silicon PV modules and guaranty conditions"

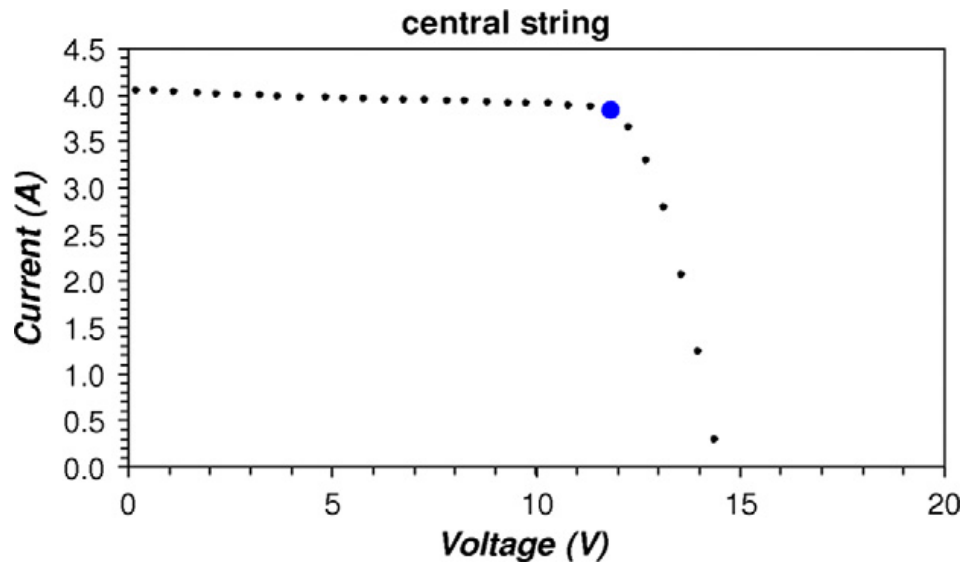


Figure 11:  $I$ - $V$  curve of the central string of cells of the module

Source: (Munoz et al. 2011) "Early degradation of silicon PV modules and guaranty conditions"

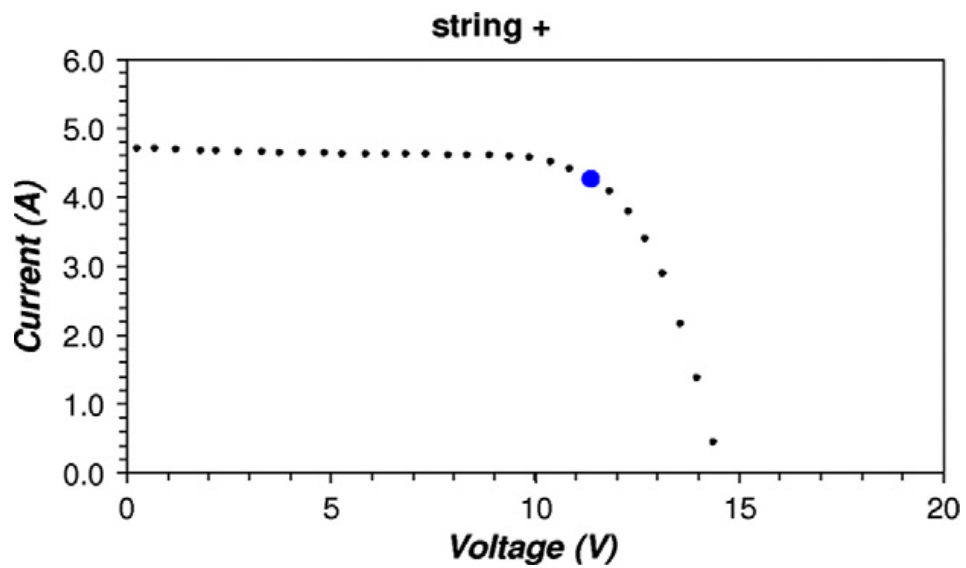


Figure 12:  $I$ - $V$  curve of the right side string of cells of the module

Source: (Munoz et al. 2011) "Early degradation of silicon PV modules and guaranty conditions"

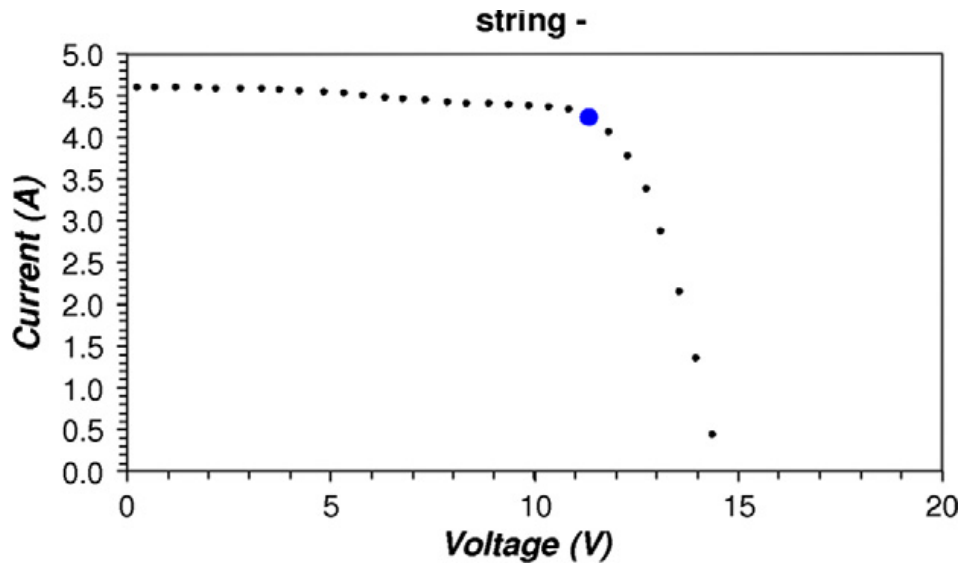


Figure 13:  $I$ - $V$  curve of the left side string of cells of the module

Source: (Munoz et al. 2011) "Early degradation of silicon PV modules and guaranty conditions"

## 2.5 Module failure

### 2.5.1 Dust and Soiling

It has been proved that dust, soiling, leaves, bird droppings, soot, snow and frost can reduce the amount of electrical current produced by PV modules. Therefore, the power output of PV modules will suffer considerable losses. Basically, all the above effects vary with local climate and tend to be seasonally dependent (Tobias 2011). Dust accumulation is largely affected by local weather patterns, local soils, air and automobile traffic, and agricultural activities. It was identified that soiling could lead to monthly power losses up to 25% and yearly losses of 7% if no proper mitigation was carried out (Tobias 2011). Therefore, regular module/array cleaning is necessary to minimize dust and soiling effects. According to recent studies, it was found that a single washing in the middle of the dry season could reduce annual dust losses by half

(from 6% to 3%) (Tobias 2011). Figure 14 illustrates dust-induced shading on PV modules.

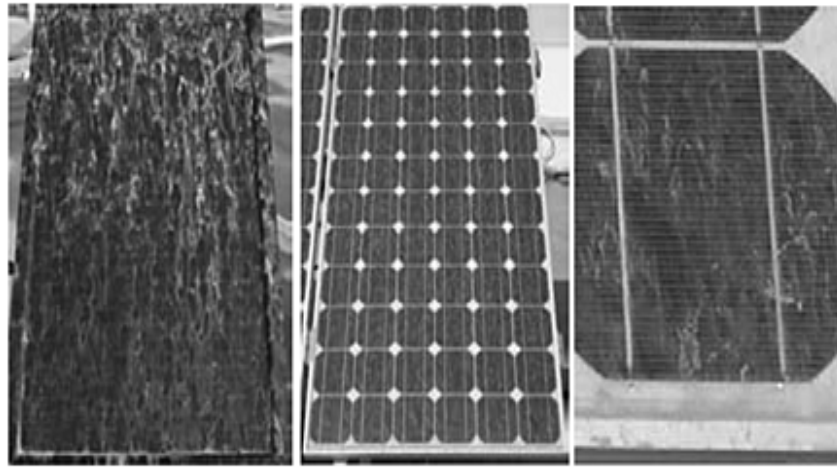


Figure 14: Dust-induced shading on PV modules

*Source: (Qasem et al. 2012) Dust-induced shading on photovoltaic modules*

### **2.5.2 Shading**

Shading is another common module failure induced by external factors (e.g. dust, tree shadings). It has been demonstrated that shade covering as little as 5-10% of an array can reduce power output by over 80% (Tobias 2011). Basically, there two types of shading: near-field shading and horizon shading.

For near-field shading, it just affects only a fraction of an array. However, horizon shading can influence either all or none of an array. The typical examples of near-field shading include local obstructions like trees and walls, and rooftop facilities. Electrically, near-field shading can be seen as a mismatch issue because if one string in a module is shaded the whole module will be shaded and the entire module can

only generate the same amount of current as its weakest string (Tobias 2011). Figure 15 shows an example of near-field shading.



Figure 15: Near-field shading induced by trees

*Source: (Emery 2011) Handbook of Photovoltaic Science and Engineering*

Horizon shading includes distant hills or some very large objects which are very close to the array such as adjacent rooftops or buildings (Tobias 2011). Horizon shading can obstruct any beam radiation from falling on the array, so a horizon-shaded array can only receive diffuse radiation. Figure 16 shows an example of horizon shading.



Figure 16: Horizon shading induced by adjacent array

*Source: (Emery 2011) Handbook of Photovoltaic Science and Engineering*

Near-field shading is complex to model but very easy to avoid. By contrast, horizon shading is simple to model but difficult or impossible to reduce. As is shown in Figure 17 and Figure 18, we can see that partial shading leads to great power losses in a crystalline silicon module whose the output dropped from 24 W to 4.8 W.

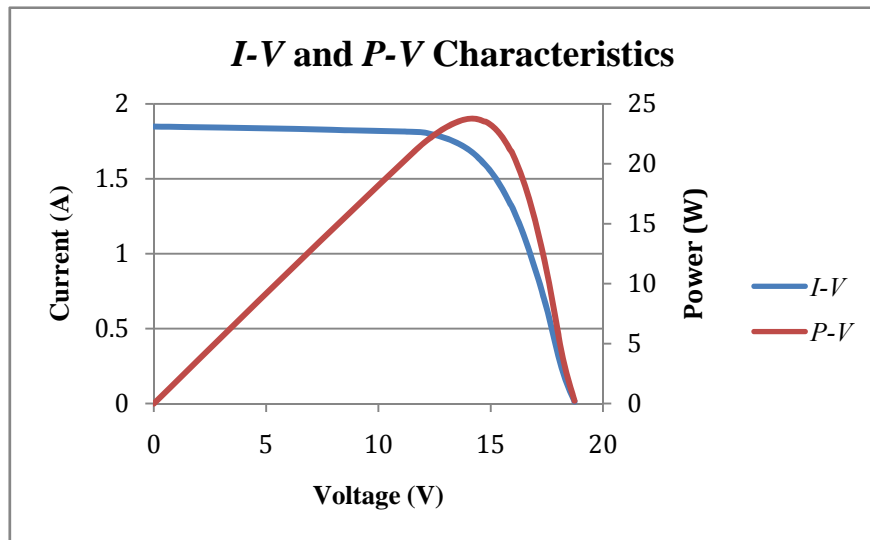


Figure 17: A crystalline module without shading

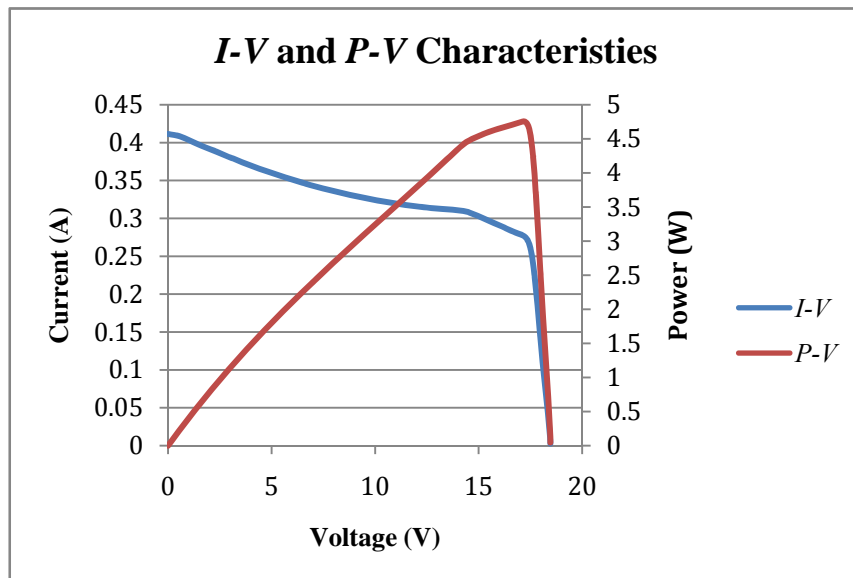


Figure 18: A crystalline module with partial shading

Source: pec621-1lab-dinz-31180265.xlsx

### **3. Troubleshooting techniques**

#### **3.1 Visual inspection**

Visual inspection, which is the first step of fault detection, allows some module degradations to be detected by sight. The method is suitable for detecting some visible defects such as yellowing, delamination, bubbles, cracks in cells, misalignments and burnt cells. Also, visual inspection can determine whether a PV module should be tested with the following procedures. The inspection must be performed under natural sunlight where PV modules can get good quality solar radiation. Furthermore, reflections should be avoided during the test because it can result in defective images. In addition, it is essential to inspect PV modules from different angles for differentiating the layer where the defects could be and avoiding the errors caused by defective images (Tobias 2011). In order to reduce detection errors, one should take a group of photos rather than a single one.

#### **3.2 Infrared imaging (IR)**

IR imaging has been considered as a common and direct technique for detecting hot spots in PV cells. This technique is based on the property that all the materials emit different electromagnetic radiation with the temperature variation of materials (Munoz 2011). During operation of a PV module, the temperature of the PV cells that have hot spot is much higher than that of normal cells. So, this temperature difference will result in two different infrared images. However, the energy that real materials

receive cannot be fully emitted and some parts of the energy will be absorbed or reflected by the air (Munoz 2011). Therefore, it is necessary to calibrate the infrared camera before taking photos. Krenzinger and Andrade (2007) recommend an accurate way of calibration that takes sky temperature and the errors caused by reflection into account (Munoz 2011). When starting to detect hot spots by using an infrared camera, one should know the ambient temperature so that one can perform corrections. Infrared cameras have advantages of high resolution and accuracy that can help us to locate the hot spot and make a comparative analysis with normal cells.

### **3.3 Lock in thermography (LIT)**

LIT is a non-destructive way to find module defects. It mainly uses injection current to detect local shunt defects. In this case, a pulsed current is injected into a solar cell. Then, the temperature increases where local shunts are situated. So, if some solar cells have shunt defects, there will be a temperature discrepancy. It is possible to adjust the injection current to measure different types of shunt defects. LIT test can be performed in dark condition (DLIT) as well as illumination condition (ILIT). In the case of ILIT, solar cells often work under open circuit conditions. By using this method, small defects can be detected because the detector is locked with bias current and it is not necessary to use high current (Munoz 2011). Normally, for taking simple IR images, the detector is a charge-coupled detector (CCD) and the range of wavelengths is 3-5  $\mu\text{m}$  because the temperature is at midrange (Munoz 2011).

### **3.4 Electroluminescence (EL) and Photoluminescence (PL) imaging techniques**

As discussed above, both IR imaging and LIT techniques are based on thermal effects. However, EL and PL imaging techniques depend on photons emitted by recombination of excited carriers in a solar cell. The Electroluminescence (EL) effect makes use of the inherent property of some materials that can emit photons in a strong electric field when injecting a current (Munoz 2011). In this case, a current is injected into the solar cells, and then initiates the EL effect. In contrast, the Photoluminescence (PL) effect occurs when those excited carriers which have absorbed photons become unstable and re-emit photons (Munoz 2011). In this case, the excitation can be achieved by incident light over the module, and light emission from the excited carriers can be detected by an infrared camera.

Although EL and PL imaging techniques use an infrared camera to take the images, the image is much better than those which use thermograph techniques. EL and PL imaging techniques are suitable to detect much smaller module defects (micro-cracks) without destroying the module. As Figure 19 shows, one string of cells reveals a darker area with the EL imaging technique, which confirms that the string has some defects due to less luminescence.

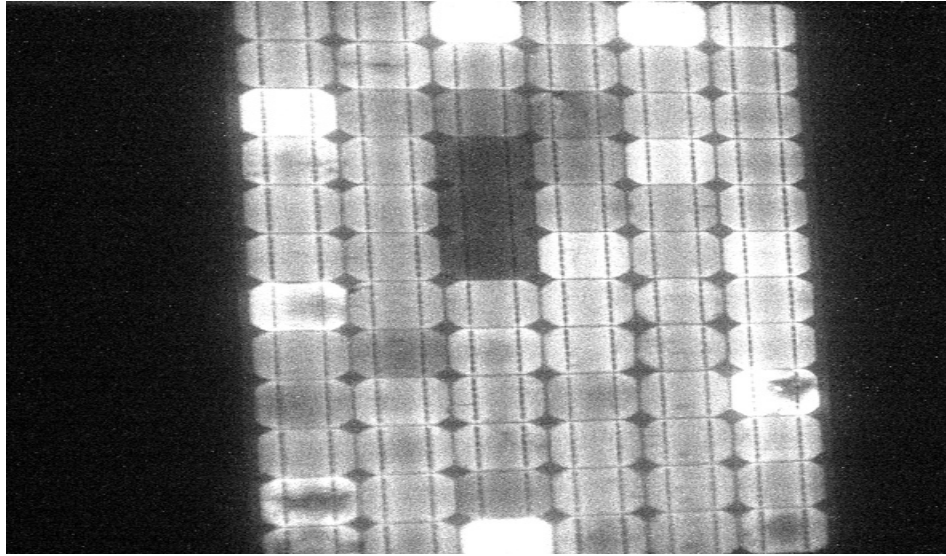


Figure 19: EL image of the previous PV module where a defect in some cells of one string of cells is confirmed

*Source: (Munoz et al. 2011) "Early degradation of silicon PV modules and guaranty conditions"*

### **3.5 Resonance ultrasonic vibrations (RUV) technique**

The RUV technique is another technique used to detect micro-cracks. It is based on the analysis of the ultrasonic vibrations that follow an excitation (Munoz 2011). Its principle is to detect the deviation of characteristic frequency of the resonance after emitting a certain ultrasonic frequency (Munoz 2011). This deviation is received by a piezoelectric transducer and transformed into electric signal, and then the electric signal is processed by a computer equipped with a data acquisition system (Munoz 2011). It has been proved that the resonant frequency drops and the bandwidth of the resonant frequency increases when a crack exists.

## **4. PV module performance measurements and degradation rate estimation**

### **4.1 Background**

It is well known that PV module performance under outdoor exposure varies with meteorological conditions. The actual output may differ from the rated output because of the wide range of temperature and solar radiation. Also, module degradation can greatly affect the actual output. Therefore, PV module performance measurement is necessary to evaluate if a module is operating properly. Normally, PV module performance is characterized by the current-voltage ( $I$ - $V$ ) testing. Under STC, the  $I$ - $V$  characteristics of a module are measured at 1000 W/m<sup>2</sup> of solar radiation, 25 °C and Airmass (AM) 1.5. However, the actual  $I$ - $V$  curves will vary under different weather conditions. In this project, four different types of PV modules: a 75W *BP275* monocrystalline module, a 75 W *SX-75* polycrystalline module, a 85W *BP585* monocrystalline module and a 70W *PW750/70* polycrystalline module are measured.

### **4.2 Description of different PV modules used in the project**

Crystalline silicon solar cells and modules have been the dominant PV technology since the beginning. Today, it is estimated that crystalline silicon occupies about 85% of the PV market (Tobias 2011). Due to different manufacturing processes, there are two major types of crystalline silicon solar cells: monocrystalline and polycrystalline

silicon. In this project, two monocrystalline silicon modules and two polycrystalline silicon modules were selected (See Figure 20).



Figure 20: Four test modules on test at ROTA

#### ***4.2.1 Monocrystalline silicon (mc-Si): BP275 & BP585***

The monocrystalline silicon solar cell is one of the most common PV technologies. Monocrystalline silicon has a pure structure without defects. In the current PV industry, the most common crystallization method is called the *Czochralski (CZ)* method. Its basic principle is to use a small polysilicon crystal properly cooled as a seed to start the crystallization process (Tobias 2011). On the one hand, this process is very slow, which increases the cost of the manufacture. On the other hand, monocrystalline silicon has a higher efficiency than polycrystalline silicon. With the

improvement of monocrystalline silicon technology, the production has become more and more cost-effective.

Two different types of monocrystalline module were selected. The first one is BP275, which is produced by the BP Solar Company. It consists of 36 series connected solar cells laminated between sheets of ethylene vinyl acetate (EVA) and high-transmissivity low-iron 3 mm tempered glass (BP Solar 2002). Its rated power output is 75W, and it can charge 12 V batteries virtually in any climate. The Electrical characteristics of the BP275 module are shown in the Table 1 below:

Table 1: BP 275 module electrical characteristics

Typical Electrical Characteristics <sup>(1)</sup>	BP 270F	BP 275F
Maximum Power ( $P_{max}$ ) <sup>(4)</sup>	70W	75W
Voltage at $P_{max}$ ( $V_{mp}$ )	17.0V	17.0V
Current at $P_{max}$ ( $I_{mp}$ )	4.16A	4.45A
Warranted minimum $P_{max}$	65W	70W
Short circuit current ( $I_{sc}$ )	4.48A	4.75A
Open-circuit voltage ( $V_{oc}$ )	21.4V	21.4V
Temperature coefficient of $I_{sc}$	(0.065±0.015)%/°C	
Temperature coefficient of $V_{oc}$	-(80±10)mV/°C	
Temperature coefficient of Power	-(0.5±0.05)%/°C	
NOCT <sup>(3)</sup>	47±2°C	
Maximum System Voltage <sup>(2)</sup>	600V	

Source: <http://www.troquedeenergia.com/Produtos/LogosModulosSolares/BP-275F.pdf>

The other type of monocrystalline module is BP585. This module is produced by the BP Solar Company as well. However, the BP585 module is different from the BP275 module because the BP Solar Company used a world leading commercial laser cell processing technology to produce the BP585 module. By using this technology, the

efficiency of the BP585 is increased to 17%, and the module surface can absorb more solar radiation and reduce reflection (BP Solar 2002). The rated output of the BP585F is 85W and it consists of 36 laser-grooved buried contact monocrystalline silicon cells. Table 2 lists its electrical characteristics:

Table 2: BP 585 module electrical characteristics

	BP 585	BP 580 <sup>†</sup>
Maximum power ( $P_{\max}$ ) <sup>2</sup>	85W	80W
Voltage at $P_{\max}$ ( $V_{mp}$ )	18.0V	18.0V
Current at $P_{\max}$ ( $I_{mp}$ )	4.72A	4.44A
Warranted minimum $P_{\max}$	80.8W	76W
Short-circuit current ( $I_{sc}$ )	5.0A	4.7A
Open-circuit voltage ( $V_{oc}$ )	22.1V	22.0V
Temperature coefficient of $I_{sc}$	(0.065±0.015)%/°C	
Temperature coefficient of voltage	-(80±10)mV/°C	
Temperature coefficient of power	-(0.5±0.05)%/°C	
NOCT <sup>3</sup>	47±2°C	
Maximum system voltage	600V (U.S. NEC rating) 1000V (TÜV Rheinland rating)	
Maximum series fuse rating	20A (U, H versions) 15A (S, L versions)	

Source: [http://www.oksolar.com/pdffiles/Solar%20Panels%20bp\\_585.pdf](http://www.oksolar.com/pdffiles/Solar%20Panels%20bp_585.pdf).

#### 4.2.2 Polycrystalline silicon (p-Si): SX-75 & PW750/70

To reduce the costs and increase the rate of production, polycrystalline silicon technology has been developed. The manufacturing process of polycrystalline silicon is simpler than that of monocrystalline silicon. One of the easiest methods to produce polycrystalline silicon is to melt the starting material (silicon scrap) and pour it into a crucible and carefully control the cooling rate (Markvart 2000). By this technology, the typical crystallization rate is 3.5kg/h, which is much faster than the CZ method (Markvart 2000).

In this project, two types of polycrystalline modules were chosen. One is a SX-75 module, which is produced by the Solarex Company. It consists of 36 series-connected polysilicon solar cells, and it can charge batteries in virtually any climate (BP Solar 2002). In addition, the rated output of the SX-75 module is 75W.

The electrical characteristics of SX-75 module are shown in Table 3:

Table 3: SX-75 module electrical characteristics

	<b>SX-75</b>	<b>SX-80</b>	<b>SX-85</b>
Maximum power ( $P_{max}$ )	75W	80W	85W
Voltage at $P_{max}$ ( $V_{mp}$ )	16.5V	16.8V	17.1V
Current at $P_{max}$ ( $I_{mp}$ )	4.54A	4.75A	4.97A
Guaranteed minimum $P_{max}$	70W	75W	80W
Short-circuit current ( $I_{sc}$ )	4.97A	5.17A	5.30A
Open-circuit voltage ( $V_{oc}$ )	20.7V	21.0V	21.3V
Maximum system voltage <sup>(2)</sup>	600V		
Temperature coefficient of $I_{sc}$	$(0.065 \pm 0.015)\%/^{\circ}\text{C}$		
Temperature coefficient of $V_{oc}$	$-(80 \pm 10)\text{mV}/^{\circ}\text{C}$		
Temperature coefficient of power	$-(0.5 \pm 0.05)\%/^{\circ}\text{C}$		
NOCT <sup>(3)</sup>	$47 \pm 2^{\circ}\text{C}$		

Source: [http://www.solarpanelsaustralia.com.au/downloads/bpsolar\\_sx80.pdf](http://www.solarpanelsaustralia.com.au/downloads/bpsolar_sx80.pdf)

The other type of module is PW750/70. This module contains  $4 \times 9$  high efficiency polycrystalline solar cells with an anti-reflective material (BP 2002). The rated power is 70W at STC. The electrical characteristics are shown in Table 4.

Table 4: PW750/70 module electrical characteristics

<b>Electrical Characteristics</b>	
STC Power Rating $P_{mp}$ (W)	70
Open Circuit Voltage $V_{oc}$ (V)	21.3
Short Circuit Current $I_{sc}$ (A)	4.50
Voltage at Maximim Power $V_{mp}$ (V)	16.7
Current at Maximim Power $I_{mp}$ (A)	4.20
Panel Efficiency	10.2%
Fill Factor	73.0%

Source: [www.posharp.com](http://www.posharp.com)

## 4.3 Major procedures

### 4.3.1 Temperature measurement

A thermocouple probe was used to measure the back of module temperature. Table 5 shows the different module temperatures measured at different times.

Table 5: Module temperature results

Module Type	PW750 /70	SX-75	BP275F	BP585
Time	Module Temperature ( $^{\circ}\text{C}$ )			
10:30 AM	29	31	31	31
11:30AM	30	30	32	40
12:30 PM	33	35	33	32
1: 30 PM	32	35	32	33
2:30 PM	35	40	37	40
3:30 PM	30	27	30	29

### 4.3.2 Solar Radiation Measurement

Solar radiation is a key parameter that can determine whether a PV module works properly. Basically, the solar radiation involves two components: direct beam and diffuse radiation. In this project, a thermopile pyranometer is mounted flat on the solar module for measuring total solar irradiance. Compared with other techniques for solar irradiance measurement, the thermopile pyranometer has significant advantages of quick response and high accuracy. However, a thermopile pyranometer should be calibrated before starting measurement, otherwise it may result in considerable errors.

#### *4.3.2.1 Pyranometer*

For maximizing the accuracy of solar irradiance readings, a Kipp&ZonenSP Lite 2 pyranometer was used to measure solar irradiance. Compared with reference cells, a Kipp&ZonenSP Lite 2 pyranometer is much more accurate and simpler to use (Appendix C). Its sensitivity is  $64.4 \mu\text{V}/\text{W}/\text{m}^2$  at normal incidence and airmass 1.5 solar irradiance, and its response time is less than 500 ns. The Kipp&Zonen SP Lite 2 pyranometer can operate under all weather conditions and the working temperature ranges from -30 C to +70 C ([www.kippzonen.com](http://www.kippzonen.com)). The calibration procedure is based on a comparison with a reference SP Lite pyranometer under artificial sun generated by an AC voltage stabilizer. This confirms that the instrument calibration factor is +1% of the stated calibration factor for an angle of incidence around 50 degrees ([www.kippzonen.com](http://www.kippzonen.com)).

#### ***4.3.3 I-V curve measurement and mapping to STC***

A Prova 210 solar module analyzer was utilized for measuring the I-V curve of the PV modules. The accuracy and reliability of this device can be found in specification sheet (Appendix D). It can be seen that both the voltage and the current should be measured within 1% and this means that the power may be calculated with 2% accuracy. In this project, the accuracy of the I-V curve testing is largely depended on the voltage and current measurements of this device, so a proper calibration is necessary to ensure that no obvious error occurs. The calibration method can be found in the measurement procedure (Appendix B).

After obtaining test results by using the Prova 210 solar module analyzer, a STC mapping spreadsheet (STC mapping tool\_master\_220611.xls at MU) was used to normalize the results to STC. This is because the electrical characteristics of modules are greatly affected by local climate conditions (temperature, solar irradiance, etc.) which means the test results are different and cannot be directly compared to previous results. Mapping testing results to STC can make all the results comparable and help to calculate the degradation rate. The specific mapping procedure is described in Appendix A.

## 5. Results and discussions

Tables 6-9 illustrate the testing results and mapping results obtained from the four different modules. Six hourly readings were taken between 10:30 AM and 3:30 PM for each module, and all the measurements were taken at the same time, and under a clear sky, to ensure no apparent error occurs. Compared with the rated output, it is found that the actual results are much lower. This demonstrates that PV modules exposed to outdoor conditions for 12 years can experience a gradual power decrease. However, it requires further analysis to calculate the exact degradation rate and examine if such a large power decrease is within the guaranteed level.

Table 6: Measured results and mapped results for PW750/70 module

Time	Temperature (°C)	Solar radiation (W/m <sup>2</sup> )	I <sub>sc</sub> -Test (A)	V <sub>oc</sub> -Test (V)	P <sub>max</sub> -Test (W)	I <sub>sc</sub> -STC (A)	V <sub>oc</sub> -STC (V)	P <sub>max</sub> -STC (W)
10:30 AM	29	970	3.523	20.19	38.5	3.57	22.65	46.25
11:30 AM	30	1043	3.83	19.98	38.27	3.61	22.3	43.82
12:30 PM	33	1060	4.23	19.39	39.02	3.91	22.61	46.96
1:30 PM	32	1050	4.094	19.59	38.42	3.83	22.53	45.77
2:30 PM	35	920	3.481	19.26	34.2	3.71	23.71	49.35
3:30 PM	30	700	2.644	19.7	29.64	3.72	23.7	50.22
AVG								47.06

Table 7: Measured results and mapped results for BP275 module

Time	Temperature (°C)	Solar radiation (W/m <sup>2</sup> )	I <sub>sc</sub> -Test (A)	V <sub>oc</sub> -Test (V)	P <sub>max</sub> -Test (W)	I <sub>sc</sub> -STC (A)	V <sub>oc</sub> -STC (V)	P <sub>max</sub> -STC (W)
10:30 AM	31	970	3.862	20.4	54.07	3.91	23.35	65.65
11:30 AM	32	1043	4.078	20.36	56.04	3.83	23.32	64.61
12:30 PM	33	1060	4.424	20	58.42	4.09	23.22	67.93
1:30 PM	32	1050	4.331	20.01	57.23	4.04	22.95	65.86
2:30 PM	37	920	3.686	19.68	49.24	3.92	24.77	70.57
3:30 PM	30	700	2.809	20.28	40.65	3.95	24.28	67.27
AVG								66.98

Table 8: Measured results and mapped results for SX-75 module

Time	Temperature (°C)	Solar radiation (W/m <sup>2</sup> )	I <sub>sc</sub> -Test (A)	V <sub>oc</sub> -Test (V)	P <sub>max</sub> -Test (W)	I <sub>sc</sub> -STC (A)	V <sub>oc</sub> -STC (V)	P <sub>max</sub> -STC (W)
10:30 AM	31	970	4.575	19.87	58.33	4.63	22.81	71.73
11:30 AM	30	1043	4.731	19.88	58.94	4.45	22.2	66.13
12:30 PM	35	1060	5.071	19.22	58.35	4.69	23.08	71.68
1:30 PM	35	1050	4.905	19.29	56.79	4.58	23.19	70.43
2:30 PM	40	920	4.253	18.94	49.57	4.52	24.99	76.35
3:30 PM	27	700	3.233	19.78	41.37	4.55	22.8	65.25
AVG								70.26

Table 9: Measured results and mapped results for BP585 module

<b>Time</b>	<b>Temperature (°C)</b>	<b>Solar radiation (W/m<sup>2</sup>)</b>	<b>I<sub>sc</sub>-Test (A)</b>	<b>V<sub>oc</sub>-Test (V)</b>	<b>P<sub>max</sub>-Test (W)</b>	<b>I<sub>sc</sub>-STC (A)</b>	<b>V<sub>oc</sub>-STC (V)</b>	<b>P<sub>max</sub>-STC (W)</b>
10:30 AM	31	970	4.645	20.33	62.98	4.7	23.27	76.86
11:30 AM	30	1043	4.557	20.24	62.84	4.29	22.56	69.97
12:30 PM	32	1060	4.88	19.8	63.66	4.52	22.7	73.26
1:30 PM	32	1050	4.692	19.83	61.72	4.36	25.32	82.2
2:30 PM	40	920	4.076	19.59	54.2	4.33	25.64	82.42
3:30 PM	29	700	3.06	20.27	44.84	4.3	23.94	73.03
AVG								76.29

Table 10: STC results and % variation in Wp over a 12-year period for four different modules

					Anna Carr's Results				Jennifer Martin's Results				A. Zendegani's Results			My Results		
Module	Cell Type	Wp Rated (W)	Wp IGM (W)	Wp Warranty Period, (W)	Wp Initial (W)	Exposure-Sure	Wp Final. Mar-02 (W)	Diff. initial to Mar-02 (%)	Exposure	Wp May-03 (W)	Wp Final, Jun-03 (W)	Diff. initial to Jun-03 (%)	Exposure	Wp Mar-07 (W)	Diff. initial to Mar-07 (%)	Exposure	Wp Aug-12 (W)	Diff. initial to Aug-12 (%)
BP2 75F	mc-Si	75	70	20yrs, 56 10yrs, 63	81.6	16 mths	78.7	-3.55	2.6 yrs	77.74	77.38	-5.17	6.4 yrs	75.81	-7.1	11.8 yrs	66.98	-17.9
BP5 85	mc-Si	85	80	20yrs, 64 10yrs, 72	86.7	13 mths	86.1	-0.69	2.3 yrs	83.74	83.1	-4.15	6.1 yrs	83.82	-3.32	11.5 yrs	76.29	-12
SX-75	p-Si	75	70	20yrs, 56 10yrs, 52	76.4	16 mths	75.3	-1.44	2.7 yrs	74.22	74.09	-3.02	6.5 yrs	72.54	-5.05	11.9 yrs	70.26	-8.04
PW 750/70	p-Si	70	65	25yrs, 52	68.6	19 mths	65.9	-3.94	3yrs	61.68	61.41	-10.48	6.7 yrs	52.86	-22.94	12.1 yrs	47.06	-31.4

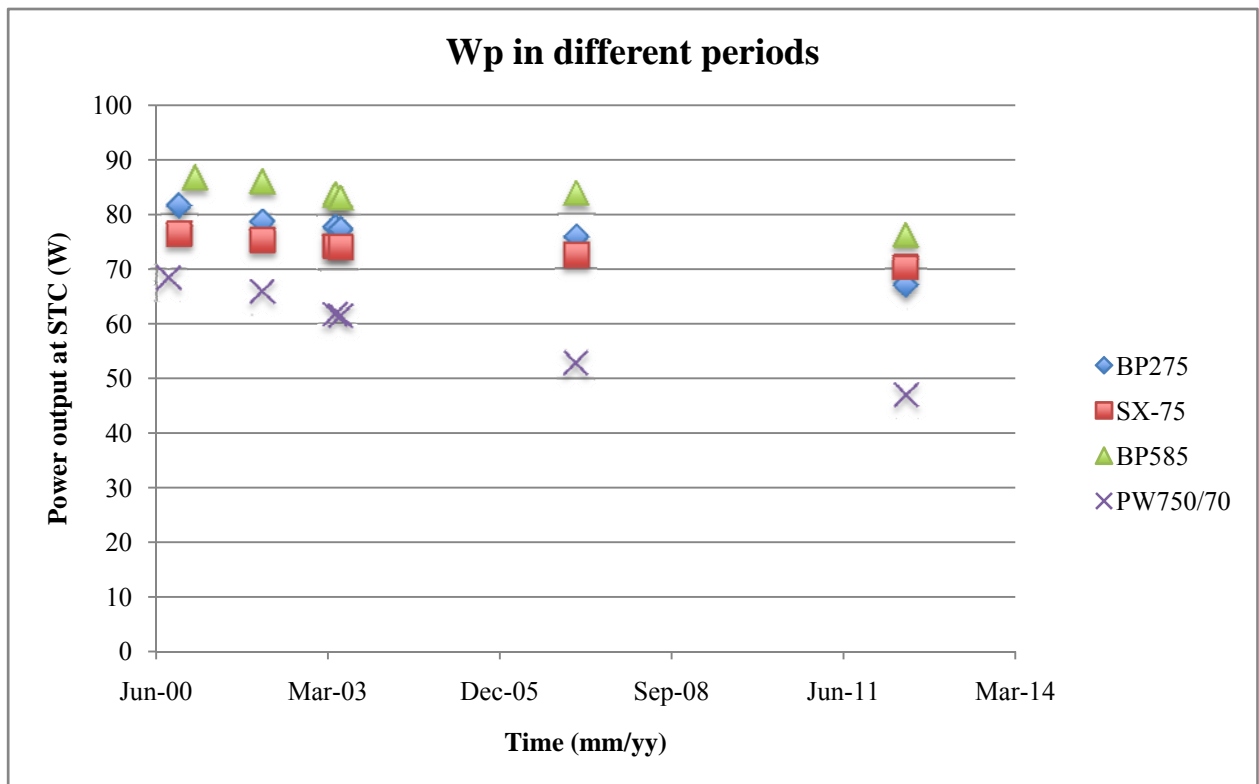


Figure 21: Power output for four different modules in different time

## 5.1 STC Test Results

Table 10 shows the rated  $W_p$ , the initial guaranteed minimum  $W_p$  (IGM) or tolerance, the initial  $W_p$  values measured prior to outdoor exposure and the  $W_p$  value measured at the end of the test period. Table 10 shows the number of months of outdoor exposure experienced by each module and the percentage differences between the initial and final  $W_p$  values. In addition, Table 10 gives us the warranty periods for each module. Due to the rapid improvement of PV technology, module warranty periods have steadily increased. Mostly, modules are guaranteed to perform to a percentage of the  $W_p$  (IGM) or a percentage of the rated power. In this project, PW750/70 module is guaranteed to perform 80% of the original  $W_p$  (IGM) after 25 years. The other three modules are guaranteed to perform at 80% of the initial  $W_p$  (IGM) after 20 years.

## 5.2 Initial STC Test Results

The initial STC test results include the initial  $W_p$  value prior to outdoor exposure and the guaranteed minimum  $W_p$  (IGM) given by the manufacturers. In most cases, the initial  $W_p$  value is higher than the  $W_p$  (IGM) and rated value even if the module has experienced one-year of outdoor exposure. In this project, we find that the initial  $W_p$  values for the SX-75 and BP585 modules are greater than their rated power (1.9% and 2.0% respectively). The initial  $W_p$  value for BP275 module is 8.8% over its rated value. However, PW750/70 module was about 2% below its rated value. This exception could result from module damage during transportation.

### 5.3 STC power after outdoor exposure

Figure 21 presents four groups of outdoor results, measured in different periods. They include three previous outdoor results provided by A. Carr, J. Martin and A. Zendegani in 2001, 2003 and 2007 respectively, and the results measured in the current study in August 2012. In order to better compare the initial results and the outdoor results, the percentage difference between the initial  $W_p$  value and the measured  $W_p$  after outdoor exposure are calculated. It was found that the  $W_p$  decrease in the four modules observed by Carr after the first 16 months of outdoor exposure agrees with those tested after 15 months of sun exposure at CH-Testing Center for PV modules, Cycle 8 project (Chianese et.al 2002). Chianese et al. (2002) noted that similar maximum power losses in almost all crystalline silicon modules range from 0.7% to 3.5% after 15 months of outdoor exposure, and the power degradation is caused by the decrease of carrier lifetime in the bulk material.

After 3-years of outdoor exposure, it can be seen that the maximum power losses of the four modules were between 3% and 11%. Although the four modules experienced a large degradation, their  $W_p$  values were still within the tolerance range provided by the manufacturers. The only exception was the PW750/70 module, which had decreased by 10.48% to a value of 3.6 W. Well below the guaranteed minimum power (IGM) of 65 W.

After 6 to 7 years of sun exposure (2007), the measured maximum power of the PW750/70 polycrystalline module was very close to its 25 year warranted minimum value of 52 W.

Compared with its initial  $W_p$  value, the measured peak power had dropped by nearly 25%. However, the two BP mc-Si modules and SX-75 (p-Si) module degraded much more slowly, by less than 9.4%. Compared with the two mono-crystalline silicon modules, the BP585 module has the lowest power loss which is less than 6%.

After about 12 years of outdoor exposure, the module degradation in these four modules continues. As is shown in the current results, the measured  $W_p$  values of the BP275 and BP585 modules had dropped by 17.9% and 12% to the values of 3.1 and 3.8 W below their IGM of 70 and 80 W. However, the two BP mc-Si modules were still in higher than their warranted values. The SX-75 polycrystalline silicon module was the only module whose power degradation is the slowest (<8.1%) after 12-years outdoor exposure, and its measured  $W_p$  value is still higher than its IGM value of 70 W.

#### **5.4 The rate of module degradation**

According to the four groups of measured results in four different periods, one can determine the changes of module performance and determine the rate of module degradation. As is shown in Figure 22, the relationship between power degradation and time fits a straight line. By using Excel 2007, one can obtain four different linear equations. The value of  $R^2$  is defined as the goodness of fit. The four linear equations have a very high  $R^2$  value (>0.86) which indicates a good correlation of maximum power with time change. The slope represents the annual power degradation. From the linear equations one can see that the two BP modules degrade 0.811W/year and 1.142 W/year respectively (BP585 and BP275). Also,

it is shown that the PW750/70 module degrades most obviously at 1.83 W/year while SX-75 module has the slowest power degradation with 0.5 W/yr. The annual degradation (W/year) is divided by the initial power output and multiplied by 100 to give the module degradation rate (%). Table 11 shows the estimated degradation rates for four different modules. Finally, it is determined that the performance of the SX-75 module is better than the other three modules, which just has degraded 0.66%/year. The BP285 module degrades 0.94%/year but is still within the 1% upper limit. By contrast, the PW750/70 module has the poorest performance with the highest degradation rate of 2.67%/year.

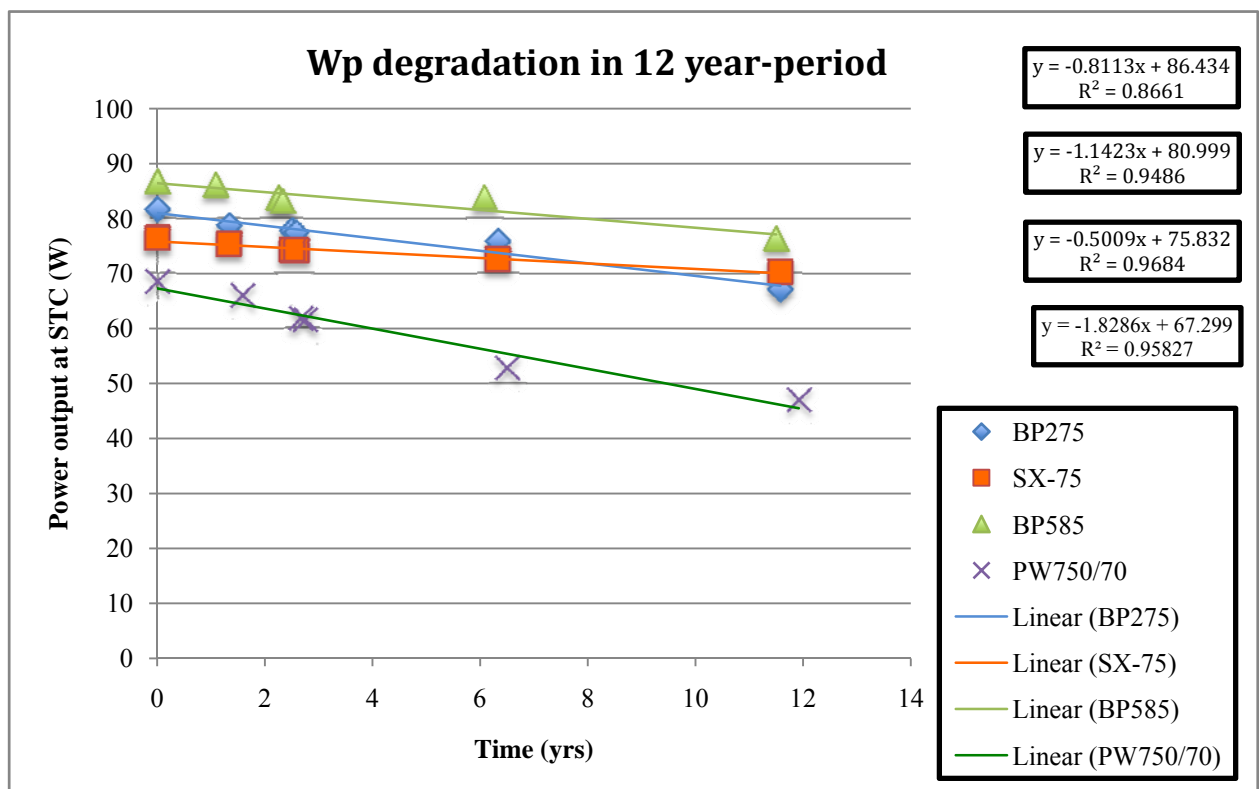


Figure 22: Power degradation with time change

Table 11: Degradation rate for four different modules

		Time (yrs)						Degradation (%)
		0	1.33	2.5	2.58	6.33	11.58	
	Rated power (W)	Power output at STC (W)						
BP 275	75	81.6	78.7	77.74	77.38	75.81	66.98	1.40
SX-75	75	76.4	75.3	74.22	74.09	72.54	70.26	0.66
		Time (yrs)						
		0	1.08	2.25	2.33	6.08	11.5	
		Power output at STC (W)						
BP285	85	86.7	86.1	83.74	83.1	83.82	76.29	0.94
		Time (yrs)						
		0	1.58	2.67	2.75	6.5	11.92	
		Power output at STC (W)						
PW750/75	70	68.4	65.9	61.68	61.41	52.86	47.06	2.67

## 6. Limitations and further research

As discussed above, the actual electrical performance of four target modules has been successfully measured and the degradation rate was estimated by comparison with previous data. However, the measured results were not verified by the simulation process because the simulator was out of service. It is suggested that a specific simulation process be conducted in future work so that it can determine if the measured results are coincident with the simulated results. Equation (3) illustrates the residual between measured results and simulated results. It is found that the less the deviation between the measured results and the simulated results, the higher the accuracy of the estimated degradation rate. The basic simulation process is to use the computer to simulate module degradation trends under STC.

The four basic simulation parameters are:  $I_{sc}$ ,  $I_{mp}$ ,  $V_{oc}$  and  $V_{mp}$ .

$$R_{pv} = \frac{|P_{mp,meas} - P_{mp,simu}|}{P_{mp,meas}} \times 100 \quad (3)$$

## **7. Conclusions and Recommendations**

PV technology has become competitive with fossil fuels in Australia due to the decreasing price and non-polluting aspects. Massive financial support and technological innovation are two big drivers that keep the PV market growing.

However, it cannot be ignored that module degradation has become a potential issue that could constrain the PV industry's development. This study summarized four basic categories of module degradation. They are cell failure, module failure, packaging material degradation and power output decrease. In addition, each category of degradation includes several different cases.

It was found that hot spot is the most common cell failure issue mainly resulting from cracked and shaded cells which can cause the overheated spot. It has been proved that solar cells that are in a long-term overheated status could experience power decrease and damage the whole structure permanently. In addition to hot spot, this study demonstrated that micro-cracks in cell could destroy the whole module structure and drastically shorten module lifecycle. Micro-cracks in cell often occur in the manufacturing process or transportation. Also, it has been seen that thermal stress and hail damage could result in micro-cracks. This study also introduces two major types of module failure caused by soiling and shading. Both types of module failure can lead to considerable power losses.

In general, module troubleshooting is divided into four steps. The first step is visual inspection in order to detect bubbles, delamination, encapsulant discoloration, glass breakage and obvious cell cracks. The next step is thermal analysis using an infrared camera to detect hot spots or an abnormal area of a module which has a much higher temperature. A bypass diode is an effective way to eliminate hot spots but it can result in extra power losses. In addition, the LIT technique combined with IR imaging is used to detect shunt defects. Further analysis consists of EL and PL imaging techniques which can detect invisible defects such as micro-cracks. Although the RUV technique has high accuracy in micro-crack detection, it is relatively expensive and complex.

The final step is outdoor PV module performance measurements. In this study, mapping measured results to STC is one of the most important steps in the outdoor PV module performance measurement because the results measured in different weather conditions are difficult to compare and need to be normalized to the same condition for comparison. In terms of the normalized results, it was found that the four measured modules have different rates of power degradation in a 12-year period. The SX-75 module is the only one whose power output is still higher than its IGM of 70 W while the other three modules have degraded below to their minimum tolerance. It was also discovered that the performance of the SX-75 module is quite good with the lowest degradation rate of 0.66 %/year while the

situation for the PW750/70 module is the worst and has resulted in considerable power losses of over 20 W, equal to a degradation rate of 2.67 %/year, after 12 years of exposure.

However, it is inevitable that experimental errors induced by changed meteorological conditions and the inaccuracy of equipments can affect the accuracy of the measured results.

So it is recommend that a specific simulation be used in future research.

## Reference

- Alers, G. B., Zhou, J., Deline, C., Hacke, P. and Kurtz, S. R. 2011. "Degradation of individual cells in a module measured with differential *IV* analysis." *Progress In Photovoltaics: Research and Application* 19: 977-982. doi: 10.1002/pip.1013.
- Boyle, G. 2004. "Solar Photovoltaics." In *Renewable Energy: Power For A Sustainable Future*, 2<sup>nd</sup>ed, edited by Godfrey Boyle. 66-104. London: Oxford University Press.
- BP Solar. 2012. Photovoltaic Module BP275 Specification Sheet.  
<http://www.troquedeenergia.com/Produtos/LogosModulosSolares/BP-275F.pdf>.  
(Accessed 14/08/2012)
- BP Solar. 2012. Photovoltaic Module SX-75, (SX-80 and SX-85) Specification Sheet.  
[http://www.solarpanelsaustralia.com.au/downloads/bpsolar\\_sx80.pdf](http://www.solarpanelsaustralia.com.au/downloads/bpsolar_sx80.pdf). (Accessed 14/08/2012)
- BP Solar. 2012. Photovoltaic Module BP585 Specification Sheet.  
[http://www.oksolar.com/pdfiles/Solar%20Panels%20bp\\_585.pdf](http://www.oksolar.com/pdfiles/Solar%20Panels%20bp_585.pdf). (Accessed 14/08/2012)
- Carr, A. J. 2005. "A detailed performance comparison of PV modules of different technologies and the implications for PV system design methods." PhD thesis, Murdoch University.
- Chianese, D., Cereghetti, N., Friesen, G., Burà, E., Realini, A., and Rezzonico, S. 2002. "Power and Energy Production of PV Modules." In *Proceeding of the: PV in Europe, from PV Technology to Energy Solutions Rome, Italy, October 2002*.  
[http://www.isaac.supsi.ch/isaac/pubblicazioni/Fotovoltaico/Conferences/Roma%20\(Italy\)%20-%20PV%20in%20Europe%20-%20October%202002/pb2.1%20power%20and%20energy%20production%20of%20pv%20modules.pdf](http://www.isaac.supsi.ch/isaac/pubblicazioni/Fotovoltaico/Conferences/Roma%20(Italy)%20-%20PV%20in%20Europe%20-%20October%202002/pb2.1%20power%20and%20energy%20production%20of%20pv%20modules.pdf). (Accessed 12/10/2012)
- Emery, K., Burdick, J., Caiyem, Y., Dunlavy, D., Field, H., Kroposki, B., Moriarty, T., Ottoson, L., Rummel, S., Strand, T. and Wanlass, M.W. 1996. "Temperature dependence of photovoltaic cells, modules and systems." In *proceeding of the 25<sup>th</sup> IEEE Photovoltaic Specialists Conference, Washington DC, May 12-17, 1996*. 1275-1278. IEEE.
- Emery, K. 2011. "Measurement and Characterization of Solar Cells and Modules." In *Handbook of Photovoltaic Science and Engineering*, 2<sup>nd</sup>ed, edited by Antonio Luque and Steven Hegedus, 797-834. A John Wiley and Sons, Ltd.

- Haberlin, H. 2010. "Solar Modules and Solar Generators." In *Photovoltaics System Design and Practice*, edited by Herbert Eppel, 127-221. A John Wiley & Sons, Ltd.
- Herrmann, W., Wiesner, W., and Vaassen, W. 1997. "Hot spot investigations on PV modules-new concepts for a test standard and consequences for module design with respect to bypass diodes." In *proceeding of the 26<sup>th</sup> IEEE Photovoltaic Specialists Conference, Anaheim, CA, September 29<sup>th</sup>-October 3<sup>rd</sup>, 1997*. 1129-1132. doi: 10.1109/PVSC.1997.654287.
- King, D. L., Quintana, M. A., Kratochvil, J. A., Ellibee, D. E. and Hansen, B. R. 2000. "Photovoltaic module performance and durability following long-term field exposure." *Progress In Photovoltaics: Research and Application* 8 (2): 241–256. doi: 10.1002/(SICI)1099-159X(200003/04)8:2<241::AID-PIP290>3.0.CO;2-D.
- Kurnik, J., Marko Jankovec, Kristijan Brecl and Marko Topic. 2011. "Outdoor testing of PV module temperature and performance under different mounting and operational conditions." *Solar Energy Materials & Solar Cells* 95: 373-376.
- Markvart, T. 2000. "Solar Cells". In *Solar Electricity*, 2<sup>nd</sup>ed, edited by Tomas Markvart, 23-79. UK: University of Southampton.
- Markvart, T. 2000. "Solar Cells." In *Solar Electricity*, 2<sup>nd</sup>ed, edited by Tomas Markvart, 23-79. UK: University of Southampton.
- Matrix Solar Technologies. 2012. Photovoltaic Module PW750/70, (PW750/80 and PW750/85) Specification Sheet.  
[http://www.altestore.com/mmsolar/others/Matrix\\_Photowatt\\_750\\_Data\\_Sheet.pdf](http://www.altestore.com/mmsolar/others/Matrix_Photowatt_750_Data_Sheet.pdf).  
 (Accessed 14/08/2012)
- Martin, J. 2003. *Training Report at MUERI*. Murdoch University Energy Research Institute.
- Munoz, M.A., Alonso-García, M.C., Nieves Vela and Chenlo, F. 2011. "Early degradation of silicon PV modules and guaranty conditions." *Solar Energy* 85 (2): 2264-2274.
- Mathew, J. K., Joseph Kuitche and Govindasamy TamizhMani. 2010. "Test-to-failure of PV modules: Hotspot testing." In *proceeding of the 35<sup>th</sup> IEEE Photovoltaic Specialists Conference, Florida, Tampa Convention Center in beautiful Tampa Bay, June 20-25, 2010*. 2839-2843. IEEE.
- McMahon, T.J. 2008. "Solar cell/module degradation and failure diagnostics." *Reliability Physics Symposium, IEEE*. 172-177. doi: 10.1109/RELPHY.2008.4558880.

- Quintana, M. A., King, D. L., McMahon, T. J. and Osterwald, C. R. 2002. "Commonly observed degradation in field-aged photovoltaic modules." In *proceeding of the 29<sup>th</sup> IEEE Photovoltaic Specialists Conference, New Orleans, Louisiana, May 19-24, 2002*. 1436-1439. IEEE.
- Roman, E., Alonso, R., Ibanez, P., Elorduizapatarietxe, S. and Goitia, D. 2006. "Intelligent PV Module for Grid-Connected PV Systems." *Industrial Electronics, IEEE Transactions* 53(4): 1066-1073, June 2006. doi: 10.1109/TIE.2006.878327.
- Takashima, T., Yamaguchi, J., Otani, K., Kato, K. and Ishida, M. 2006. "Experimental Studies of Failure Detection Methods in PV Module Strings." In *proceeding of the 4<sup>th</sup> World Photovoltaic Energy Conversion Conference, May 7-12, 2006*. 2227-2230. doi: 10.1109/WCPEC.2006.279952.
- Tobias, I., Carlos del Canizo and Jesus Alonso. 2011. "Crystalline Silicon Solar Cells and Modules." In *Handbook of Photovoltaic Science and Engineering*, 2<sup>nd</sup>ed, edited by Antonio Luque and Steven Hegedus, 265-308. A John Wiley and Sons, Ltd.
- Thomas, M. G., Durand, S. J., and Rosenthal, A. L. 1993. "A Ten-Year Review of Performance of Photovoltaic Systems." In *Proceedings of the 23<sup>rd</sup> Photovoltaic specialists Conference*, Louisville, KY, May 10-14, 1993. IEEE.
- Whitaker, C. M., Townsend, T. U., Anat Razon, Hudson, R. M. and Xavier Vallve. 2011. "PV Systems." In *Handbook of Photovoltaic Science and Engineering*, 2<sup>nd</sup>ed, edited by Antonio Luque and Steven Hegedus, 797-834. A John Wiley and Sons, Ltd.
- Yanli Liu, Bingfeng Li, and Dan Zhong. 2010. "Research on Domestic PV Module Structure Based on Fault Detection." In *Proceedings of the 8<sup>th</sup> World Congress on Intelligent Control and Automation, Jinan, China, July 6-9, 2010*. 171-175. IEEE.

## Appendices

### Appendix A

#### Procedure for converting the IV Curve measured in the field to STC using STC Mapping Spreadsheet

##### Definitions

AOI	Angle of incidence between beam from sun and normal to array plane.
$\alpha_{Imp}$	Module $I_{mp}$ temperature coefficient, normalized, (1/C)
$\alpha_{Isc}$	Module $I_{sc}$ temperature coefficient, normalized, (1/C)
$\beta V_{mpo}$	Module $V_{oc}$ temperature coefficient at 1000 W/m <sup>2</sup> , (V/C)
$\beta V_{oco}$	Module $V_{oc}$ temperature coefficient at 1000 W/m <sup>2</sup> , (V/C)
$I_{mpo}$	$I_{mp}$ at STC (A)
$I_{sco}$	$I_{sc}$ at STC (A)
RRPGP	In this document refers to the project of 1 <sup>st</sup> semester 2011 funded by RRPGP.
SMD	Sandia Module Database
STCMS	STC mapping spreadsheet
$V_{mpo}$	$V_{mp}$ at STC (V)
$V_{oco}$	$V_{oc}$ at STC (V)

Step 1. Check that PV module is in the SMD and copy and paste into STCMS.

The STCMS uses the model as outlined in King, Boyson, and Kratochvil (2004). As such it relies on the SMD for solar module characteristics. Therefore the solar array being mapped must contain modules that are included in the SMD. For the RRPGP, a match was judged as exact if the model number was basically the same as that listed in the SMD and the  $V_{oc}$ ,  $I_{sc}$ ,  $V_{mpo}$ ,  $I_{mpo}$  figures given on the module label matched exactly those listed in the SMD. Sometimes an exact match was not found. Where an exact match was not found a module was selected from the same family with similar  $V_{oc}$ ,  $I_{sc}$ ,  $V_{mpo}$  &  $I_{mpo}$ . These figures were then adjusted to exactly reflect those given on the module label. Further validation of this method could be conducted by sourcing the original datasheet for each module. Figures for  $\alpha_{Isc}$ ,  $\beta V_{oco}$ , and the power temperature coefficient are commonly supplied on datasheets. These figures can be checked against the  $\alpha_{Isc}$ ,  $\beta V_{oco}$ ,  $\alpha_{Imp}$ , and  $\beta V_{mpo}$  given on the SMD. This extra validation was conducted on one module type (BP480H) in the RRPGP because the nearest match on the SMD appeared such that it may not have

been sufficiently similar to the BP480H module. It took great effort to extract the correct datasheet for BP480H from the PV manufacturer.

One module label only carried Vmpo & Impo information (not Voco & Isco). Because the module number was a reasonable match to the SMD and Vmpo and Impo were exact matches it is likely that the SMD entry chosen, accurately reflected the module in question. As an extra precaution the datasheet was requested from the manufacturer with the following reply after a long delay and a reminder.

Given the author's experience with BP and Sharp, the reluctance of manufacturers to maintain and supply data on PV modules of a reasonable age adds to difficulties in assessing degradation.

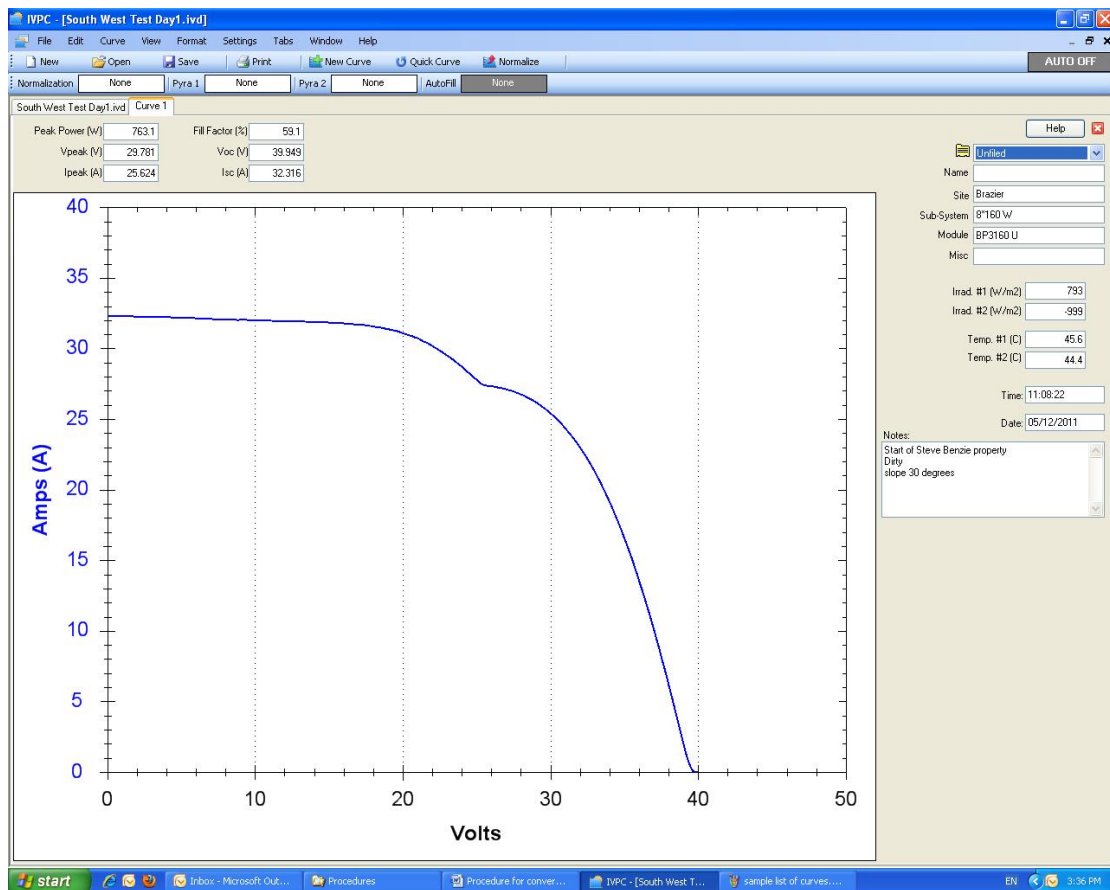
Open the STCMS (STC mapping tool\_master\_220611.xls) and save it with an appropriate filename for the curve or curves being mapped. Open the SMD in excel and copy the row corresponding to the PV module being tested. Paste this row into the STCMS at row 5. If the SMD entry is not an exact match to the module label (as described above) then the appropriate figures should be adjusted in the spreadsheet at this stage.

Step 2. Enter the system commissioning date in row 7.

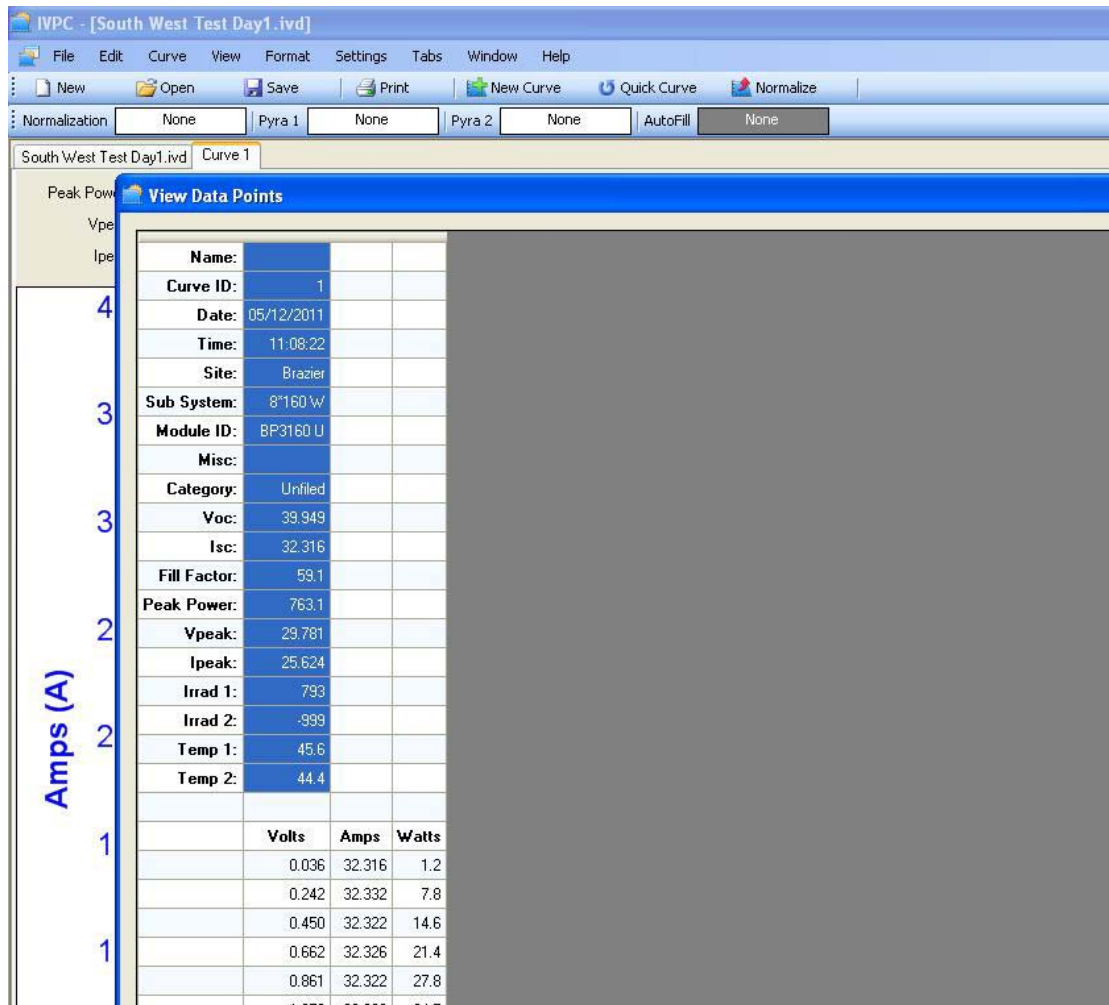
Step 3. The Daystar IV curve tracer produces a file with extension ".ivd". This file must be opened using the Daystar IV curve tracer software. Resulting in a display like that below.

IVPC - [South West Test Day1.ivd]									
File Edit Curve View Format Settings Tabs Window Help									
New Open Save Print New Curve Quick Curve Normalize									
Normalization None Pyra 1 None Pyra 2 None AutoFill None									
South West Test Day1.ivd									
	CurveID	Normalized	Category	Name	Site	Sub System	Module	Misc	Date/Time
<input checked="" type="checkbox"/>	1		Unfiled		Brazier	8"160 W	BP3160 U		05/12/2011 11:08:22
<input type="checkbox"/>	2		Unfiled		Brazier		BP3160 U		05/12/2011 11:11:00
<input type="checkbox"/>	3		Unfiled		Brazier		BP3160 U		05/12/2011 11:12:00
<input type="checkbox"/>	4		Unfiled		Brazier		BP3160 U		05/12/2011 11:13:00
<input type="checkbox"/>	5		Unfiled		Brazier		BP3160 U		05/12/2011 11:14:00
<input type="checkbox"/>	6		Unfiled		Brazier		BP3160 U		05/12/2011 11:15:00
<input type="checkbox"/>	7		Unfiled		Brazier		BP 3160U		05/12/2011 11:16:00
<input type="checkbox"/>	8		Unfiled		Brazier		BP 3160U		05/12/2011 11:17:00
<input type="checkbox"/>	9		Unfiled		Brazier		BP 3160U		05/12/2011 11:18:00
<input type="checkbox"/>	10		Unfiled		Brazier		BP 3160U		05/12/2011 11:19:00
<input type="checkbox"/>	11		Unfiled		Brazier		BP 3160U		05/12/2011 11:20:00
<input type="checkbox"/>	12		Unfiled		Brazier		BP 3160U		05/12/2011 11:36:17
<input type="checkbox"/>	13		Unfiled		Brazier		BP 3160U		05/12/2011 11:37:00
<input type="checkbox"/>	14		Unfiled		Brazier		BP 3160U		05/12/2011 11:38:01
<input type="checkbox"/>	15		Unfiled		Brazier		BP 3160U		05/12/2011 11:39:00
<input type="checkbox"/>	16		Unfiled		Brazier		BP 3160U		05/12/2011 11:40:00
<input type="checkbox"/>	17		Unfiled		Brazier		BP3160U		05/12/2011 11:41:00
<input type="checkbox"/>	18		Unfiled		Brazier		BP3160U		05/12/2011 11:42:03
<input type="checkbox"/>	19		Unfiled		Brazier		BP 3160U		05/12/2011 11:43:00
<input type="checkbox"/>	20		Unfiled		Brazier		BP 3160 U		05/12/2011 11:44:00
<input type="checkbox"/>	21		Unfiled		Brazier		BP 3160 U		05/12/2011 11:45:00
<input type="checkbox"/>	22		Unfiled		Forrest Road	16"80W	BP 480H		05/12/2011 13:43:47
<input type="checkbox"/>	23		Unfiled		Forrest Road		BP 480H		05/12/2011 13:45:00
<input type="checkbox"/>	24		Unfiled		Forrest Road		BP 480H		05/12/2011 13:46:00
<input type="checkbox"/>	25		Unfiled		Forrest Road		BP 480H		05/12/2011 13:47:00
<input type="checkbox"/>	26		Unfiled		Forrest Road		BP 480H		05/12/2011 13:48:00
<input type="checkbox"/>	27		Unfiled		Forrest Road		BP 480H		05/12/2011 13:49:00

Step 4. Double click on the curve which needs to be mapped to STC to open the curve window as seen below.



Step 5. Press control 'D' to display the curve data and select the required data as shown below (selected section in blue).



Step 6. Press control 'C' to copy data. Open STC mapping spreadsheet (STC mapping tool\_master\_220611.xls) and save it under an appropriate name for the curve being mapped. Paste data into area adjacent to yellow highlighted area as shown below. The yellow area is the original reference calculation and formulas which must remain untouched.

STC mapping tool_master_220611.xls [Compatibility Mode] - Microsoft Excel									
<div> <div>Home Insert Page Layout Formulas Data Review View Add-Ins</div> <div> <div> <div>Cut Copy Paste</div> <div>Format Painter</div> <div>Clipboard</div> </div> <div> <div>Calibri 11</div> <div> <div></div> <div></div> <div></div> </div> <div> <div></div> <div></div> <div></div> </div> </div> <div> <div>Wrap Text</div> <div>Merge &amp; Center</div> </div> <div> <div>General</div> <div>\$ %</div> <div>0.00 0.00</div> </div> <div> <div>Conditional Formatting</div> <div>Format as Table</div> <div>Cell Styles</div> </div> <div> <div>Insert</div> </div> </div> </div>									
D17									
	A	B	C	B	C	D	E		
1	Notes								
2									
3	INPUTS								
4	Model	Vintage	Area	Vintage	Area	Material	Series_Cells	Par	
5	BP Solar BP380 [2006 (E)]	2006 (E)	0.649	2006 (E)	0.649	mc-Si	36		
6									
7	System commissioning date (mm/dd/year)	30/01/2005		30/01/2005					
8									
13	q (coulomb)	1.602180E-19	1.602180E-19	1.602180E-19	1.602180E-19	1.60218E-19	1.60218E-19	1.	
14	k (J/K)	1.380660E-23	1.380660E-23	1.380660E-23	1.380660E-23	1.38066E-23	1.38066E-23	1.	
15									
16	COPY & PASTE FROM IVPC								
17	Name:								
18	Curve ID:	REF		REF		1			
19	Date (need to change from US to AUS notation):	12/05/2011		12/05/2011		5/12/2011			
20	Time:	11:08:22		11:08:22		11:08:22			
21	Site:	Brazier		Brazier		Brazier			
22	Sub System:	8*160 W		8*160 W		8*160 W			
23	Module ID:	BP3160 U		BP3160 U		BP3160 U			
24	Misc:								
25	Category:	Unfiled		Unfiled		Unfiled			
26	Voc:	39.949		39.949		39.949			
27	Isc:	32.316		32.316		32.316			
28	Fill Factor:	59.1		59.1		59.1			
29	Peak Power:	763.1		763.1		763.1			
30	Vpeak:	29.781		29.781		29.781			
31	Ipeak:	25.624		25.624		25.624			
32	Irrad 1:	793		793		793			
33	Irrad 2:	-999		-999		-999			
34	Temp 1:	45.6		45.6		45.6			
35	Temp 2:	44.4		44.4		44.4			
36									
37	Percent diffuse assumption	10%		10%		10%		10%	

Step 7. If more than one curve was taken with the same array then repeat from step 4 pasting into adjacent columns as shown below. In the RRP GP usually ten curves had been taken 1 minute apart. When first pasted, the date format is mm/dd/yyyy and this must be manually changed to dd/mm/yyyy on each column.

STC mapping tool_master_220611.xls [Compatibility Mode] - Microsoft Excel									
Home Insert Page Layout Formulas Data Review View Add-Ins									
Clipboard Font Alignment Number Styles Cells									
F17 fx									
	A	B	C	B	C	D	E	F	
1	Notes								
2									
3	INPUTS								
4	Model	Vintage	Area	Vintage	Area	Material	Series_Cells	Parallel_C-S	Isc
5	BP Solar BP380 [2006 (E)]	2006 (E)	0.649	2006 (E)	0.649	mc-Si	36	1	
6									
7	System commissioning date (mm/dd/year)	30/01/2005		30/01/2005					
8									
13	q (coulomb)	1.602180E-19	1.602180E-19	1.602180E-19	1.602180E-19	1.60218E-19	1.60218E-19	1.60218E-19	1.6
14	k (J/K)	1.380660E-23	1.380660E-23	1.380660E-23	1.380660E-23	1.38066E-23	1.38066E-23	1.38066E-23	1.3
15									
16	COPY & PASTE FROM IVPC								
17	Name:								
18	Curve ID:	REF		REF		1	2	3	
19	Date (need to change from US to AUS notation):	12/05/2011		12/05/2011		5/12/2011	5/12/2011	5/12/2011	
20	Time:	11:08:22		11:08:22		11:08:22	11:11:00	11:12:00	
21	Site:	Brazier		Brazier		Brazier	Brazier	Brazier	
22	Sub System:	8*160 W		8*160 W		8*160 W			
23	Module ID:	BP3160 U		BP3160 U		BP3160 U	BP3160 U	BP3160 U	
24	Misc:								
25	Category:	Unfiled		Unfiled		Unfiled	Unfiled	Unfiled	
26	Voc:	39.949		39.949		39.949	39.831	39.932	
27	Isc:	32.316		32.316		32.316	32.619	32.757	
28	Fill Factor:	59.1		59.1		59.1	59	58.9	
29	Peak Power:	763.1		763.1		763.1	765.9	769.9	
30	Vpeak:	29.781		29.781		29.781	29.553	29.708	
31	Ipeak:	25.624		25.624		25.624	25.918	25.915	
32	Irrad 1:	793		793		793	822	812	
33	Irrad 2:	-999		-999		-999	-999	-999	
34	Temp 1:	45.6		45.6		45.6	46.4	46.2	
35	Temp 2:	44.4		44.4		44.4	45.7	45.1	
36									
37	Percent diffuse assumption	10%		10%		10%	10%	10%	

Step 8. Once all the curves are entered into the STCMS. Ensure a figure for percent diffuse is in each relevant column for row 37.

Step 9. Enter latitude and longitude in rows 40-43.

Step 10. AOI

If the array is on a tracker then AOI is best measured directly before commencing taking of curves. In this case the measured AOI must overwrite the formula in row 73 and no data needs to be entered in row 44&45. AOI was assumed constant for all curves taken within 20 minutes. This was the method used for arrays mounted on trackers in RRP GP.

If the array is fixed then the STCMS calculates AOI from rows 44 to 47 which must be entered. In RRP GP Solar elevation and solar azimuth (row 46 & 47) were calculated using the website: <http://www.srrb.noaa.gov/highlights/sunrise/azel.html> with offset to UTC -8 and manually entering the latitude, longitude, date, and time information.

Anecdotal sensitivity analysis revealed that results were unaffected by assuming the sun position remained constant for up to 20 minutes. Therefore, a single value for sun position was entered in to row 46&47 across all curves as long as the curves were all taken within 20 minutes.

Step 11. A figure for altitude must be entered in row 48. RRP GP used google earth data for this.

Step 12. Length of string (row 51) and Number of strings (row 52) must be entered. If this is incorrect it results in obvious but not real degradation figures further down the spreadsheet.

Step 13. Below row 57 is the STCMS outputs so no more data is required to be entered below this row. The formulas may need to be copied and dragged across from the reference column c so that each curve has its own calculations. Degradation figures can be gleaned from rows 112 to 118. It is a good idea to check that degradation is similar across all curves in the spreadsheet. Rounded degradation figures typically varied by +/-1% in the RRP GP. Occasional outliers beyond this were removed. Sometimes variability exceeded this value and outliers could not be identified. Such data was deemed bad data and could not be used. This was found to occur when we were attempting to take curves in a short break (<10mins) in the clouds. Variability in the fill factor figures occurred to a much lower extent than in the power degradation figures.

## **Appendix B**

### **Procedures of Prova 210 Solar *I-V* Tracer**

- 1) Attach the temperature sensing element of the temperature probe to the back of the solar module using the aluminium tape to get the most approximate temperature at the back of the module (For achieving the best results, we can use a 15 mm×100 mm piece of A1 tape to attach the temperature probe to the back of the module).
- 2) Calibrate the voltage and current and press the "ZERO CAL" button (It can improve the accuracy of the instrument before operation).
- 3) Connect the PV module to the solar module analyzer using the leads (Plug the red and black leads into the mating connectors of Prova 210; then connect the negative lead to the PV module followed by the positive red lead).
- 4) Press the power button of the Prova 210 to switch the unit on.
- 5) Setup menu to 0 minutes and input the measured module area, solar radiation.
- 6) Press the AUTO SCAN button and all the measured data will be transformed into a I-V&P-V curve, then store the data pressing the REC button and note the record number.
- 7) Connect the solar analyzer to the computer and start the "Solar Module Analyzer 12A" software.
- 8) Click the "Communication" button.
- 9) Select "REC/LOAD" to download the recording.
- 10) Click on "Export to Excel" to save all records in .csv format.
- 11) Click on "Clear" to delete the records from the unit for the next students.

## Appendix C

### Pyranometers v. Reference Cells for PV Installations

Advantages of a pyranometer over a reference cell:

1. The pyranometer gives an independent, accurate reading of the total available solar radiation
2. The pyranometer are classified and calibrated to ISO standards
3. The response time of the pyranometer is longer than a PV cell
4. The pyranometer is PV cell type independent
5. A pyranometer can have a very small temperature coefficient
6. PV cells are specified at STC (Standard Test Conditions)
7. Reference cells (and PV panels) suffer more from pollution than pyranometers
8. Performance Ratio or Performance Index calculations are more accurate using a pyranometer

Explanations of the above advantages:

Advantage 1: Depending on the technology (amorphous silicon, thin film CdTe or triple-junction cells, etc) and the cell/panel 'window' material PV cells have different spectral responses. Due to the changing position of the sun (Air Mass), pollution, humidity, clouds, etc., the solar spectrum at ground level varies considerably.

Advantage 2: Pyranometers measure the total solar spectrum from 0.3 to 3 micrometers wavelength and give an integrated measurement of the total short-wave solar energy available under all conditions. Pyranometers have been the instruments used to measure solar radiation for over 80 years. The worldwide solar radiation database is founded on pyranometer measurements. Also the pyranometer calibration factor is very stable over time. Performance classifications are defined by ISO 9060 and the calibration methods by ISO 9847.

Advantage 3: The advantage here is that the pyranometer integrates over time, typically between 5 and 20 seconds. This means that sudden changes such as passing small clouds, birds and planes will not give transient spikes or dips in the data.

A pyranometer will give a correct integrated values over a day when using sample intervals of 20 seconds or more.

Advantage 4: When different PV cell types are used in one plant, a separate reference cell for each type should be used, but only one pyranometer is required for monitoring all types.

Advantage 5: The temperature dependency of pyranometers can be as low as 1 % over a 70 °C temperature range (depending on type). This is much lower than that of PV panels and reference cells.

Advantage 6: Most panels and reference cells have performance are specified under Standard Test Conditions. These are conditions of +25°C ambient temperature, 1000W/m<sup>2</sup> global solar irradiance, air mass 1.5 and no wind. The global radiation when under test is measured with a pyranometer. These conditions are far from realistic in the real world and an accurate measurement with a pyranometer shows the real performance.

Advantage 7: There is a conception that pyranometers need to be cleaned very frequently, and this is advised for optimum performance. However, reference cells with a flat surface suffer more from deposits than the hemi-spherical dome of a pyranometer.

Advantage 8: Performance Ratio (PR) or Performance Index (PI) calculations when based on accurate independent data from a pyranometer are more relevant than when based on a reference cell with lower accuracy and the same inherent flaws as the panel itself. A pyranometer (depending on the type) can measure with 1% accuracy.

## Appendix D

### Prova 210 Solar Module Analyzer Accuracy and Reliability

**PROVA®**

**PROVA 200** Solar Module Analyzer (6A / 60V)  
**PROVA 210** Solar Module Analyzer (12A / 60V)

#### Electrical Specifications: (23°C±5°C, Four-wire Measurement)

##### PROVA 200

###### DC Voltage Measurement

Range	Resolution	Accuracy
0 ~ 6 V	0.001 V	± 1 % ± (1 % of Vopen ± 9mV)
6 ~ 10 V	0.001 V	± 1 % ± (1 % of Vopen ± 0.09V)
10 ~ 60 V	0.01 V	± 1 % ± (1 % of Vopen ± 0.09V)

###### DC Current Measurement

Range	Resolution	Accuracy
0.01 ~ 0.6 A	0.1 mA	± 1 % ± (1 % of Ishort ± 0.9mA)
0.6 ~ 1 A	0.1 mA	± 1 % ± (1 % of Ishort ± 9mA)
1 ~ 6 A	1 mA	± 1 % ± (1 % of Ishort ± 9mA)

##### PROVA 200-24

###### DC Voltage Measurement

Range	Resolution	Accuracy
0 ~ 1 V	0.001 V	± 1 % ± (1 % of Vopen ± 9mV)
1 ~ 24 V	0.01 V	± 1 % ± (1 % of Vopen ± 0.09V)

###### DC Current Measurement

Range	Resolution	Accuracy
0 ~ 60 mA	0.01 mA	± 1 % ± (1 % of Ishort ± 90µA)
60 ~ 100 mA	0.01 mA	± 1 % ± (1 % of Ishort ± 0.9mA)
100 ~ 600 mA	0.1 mA	± 1 % ± (1 % of Ishort ± 0.9mA)

##### PROVA 210

###### DC Voltage Measurement

Range	Resolution	Accuracy
0 ~ 10 V	0.001 V	± 1 % ± (1 % of Vopen ± 0.1 V)
10 ~ 60 V	0.01 V	± 1 % ± (1 % of Vopen ± 0.1 V)

###### DC Current Measurement

Range	Resolution	Accuracy
0.01 ~ 10 A	1 mA	± 1 % ± (1 % of Ishort ± 9 mA)
10 ~ 12 A	10 mA	± 1 % ± (1 % of Ishort ± 0.09A)

#### General Specifications:

AC Adaptor:	AC 110V or 220V input, DC 12V / 1~3A output
Operation Environment:	0°C ~ 50°C, 85% RH
Storage Environment:	-20°C ~ 60°C, 75% RH
Weight:	1160g / 40.9oz (Batteries included)
Dimension:	257(L) x 155(W) x 57(H) mm 10.1" (L) x 6.1" (W) x 2.2" (H)
Accessories:	User Manual x 1, AC adaptor x 1 Software CD x 1, Software Manual x 1 RS232C (to USB Bridge) Cable x 1 Kelvin Clips (2 clips) x 1 set 210: Lithium battery 11.1V (Rechargeable) x 1 200: Battery 1.2V AA (Rechargeable) x 8

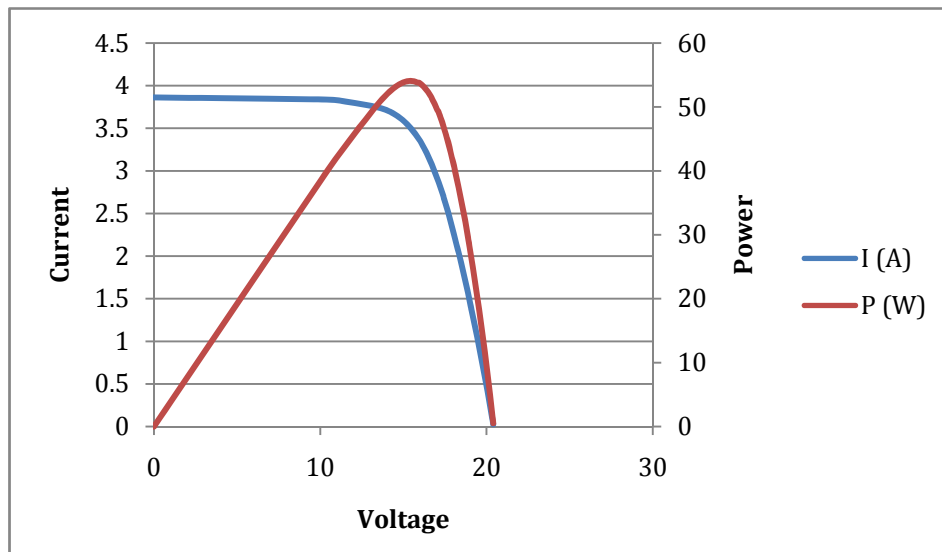


**SALES**  
 PH: 1300 853 407  
 FAX: 1300 853 409  
[sales@triosmartcal.com.au](mailto:sales@triosmartcal.com.au)

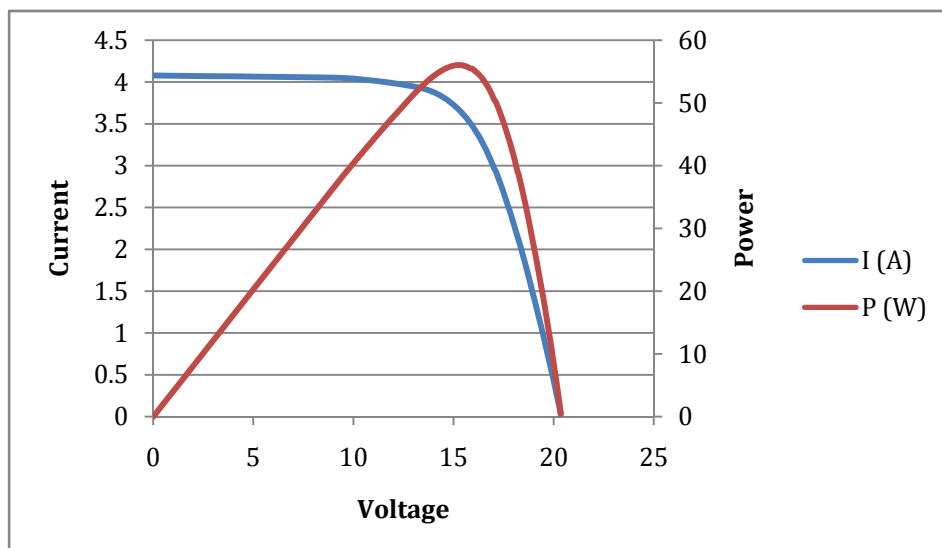
**SERVICE**  
 PH: 1300 134 091  
 FAX: 1300 134 099  
[service@triosmartcal.com.au](mailto:service@triosmartcal.com.au)

## Appendix E

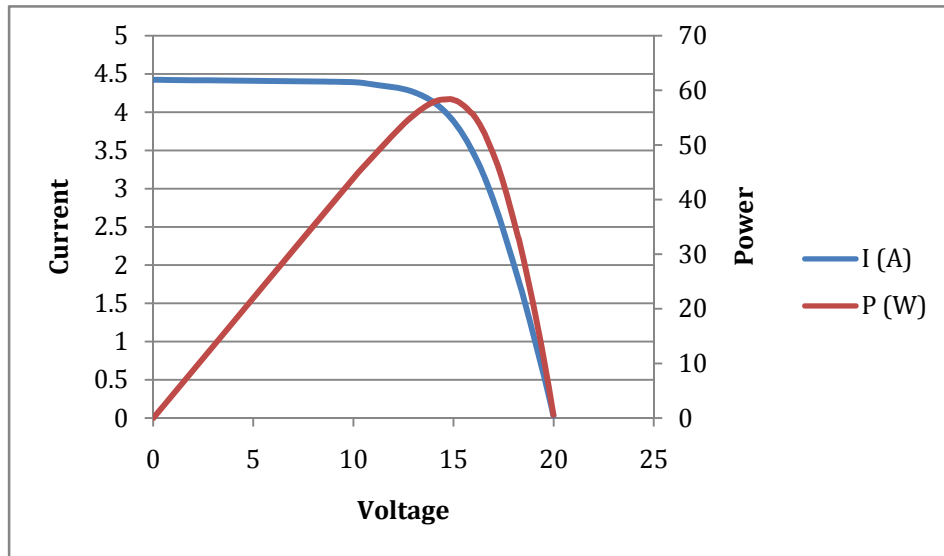
### Comparison of $I$ - $V$ curves for different modules under different times of the day



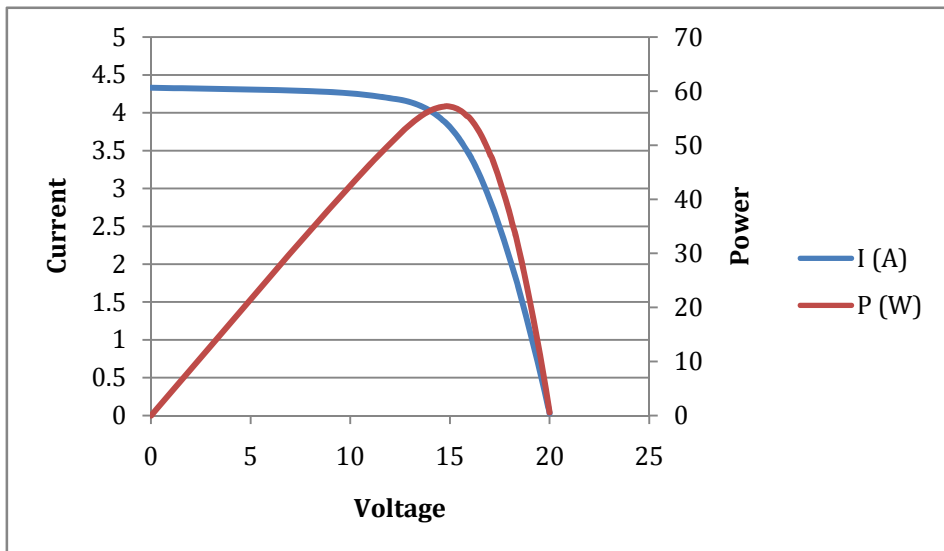
BP275 Module at 970 W/m<sup>2</sup>, 31°C (10:30 AM)



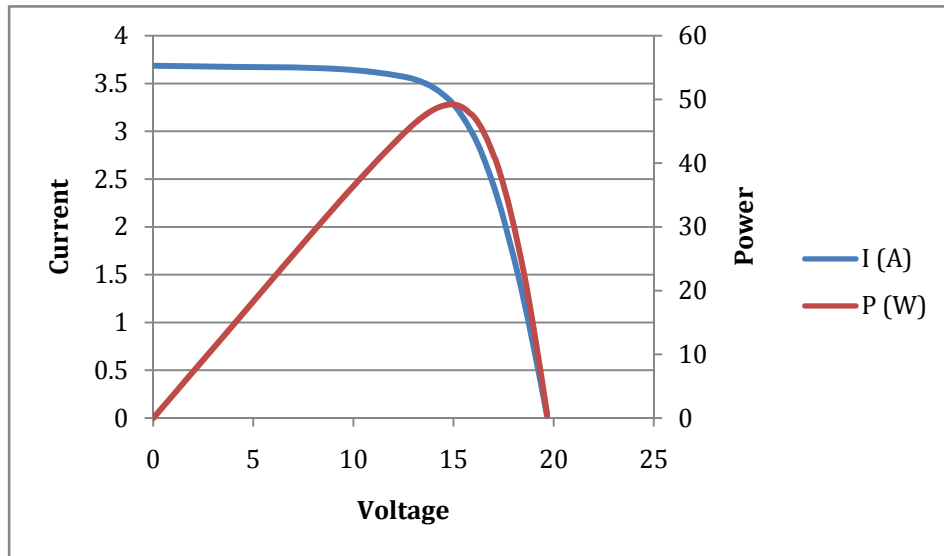
BP275 Module at 1043 W/m<sup>2</sup>, 32°C (11:30 AM)



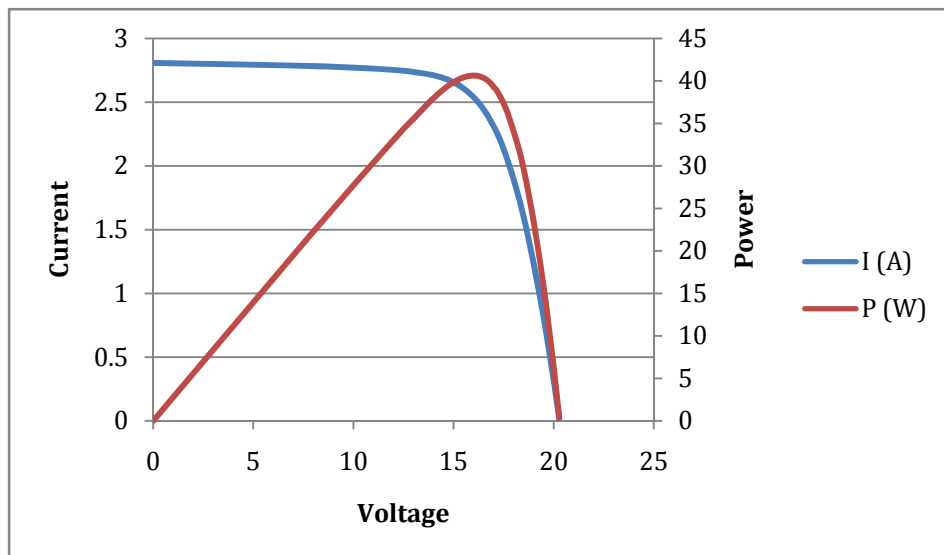
**BP275 Module at 1060 W/m<sup>2</sup>, 33°C (12:30 PM)**



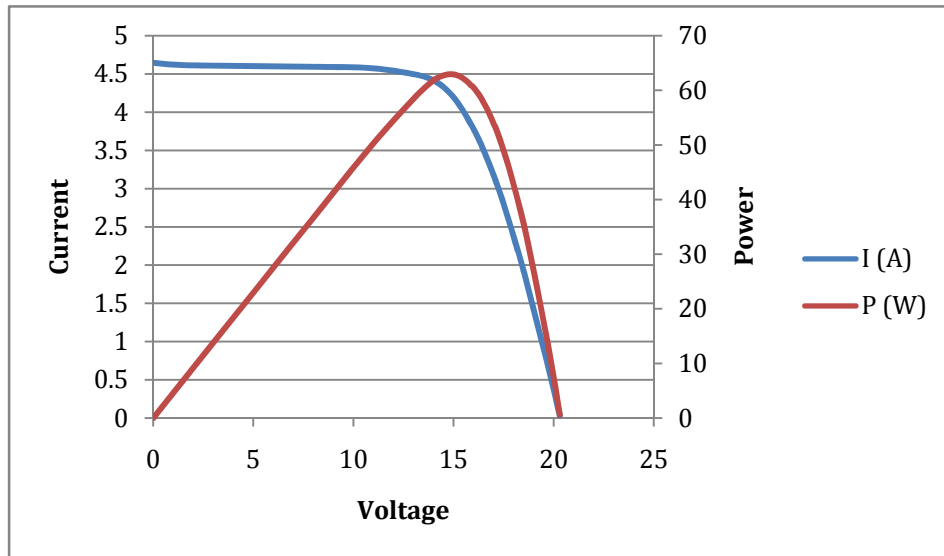
**BP275 Module at 1050 W/m<sup>2</sup>, 32°C (1:30 PM)**



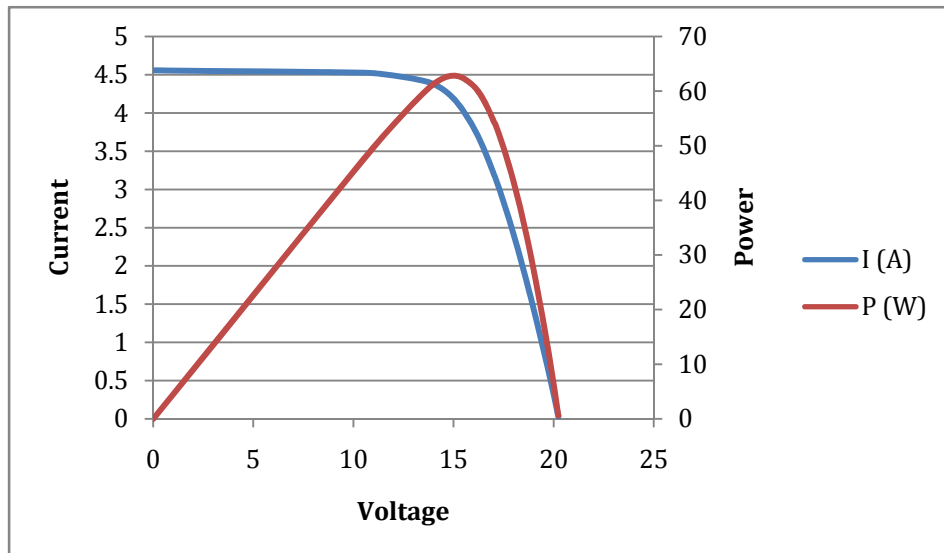
**BP275 Module at 920 W/m<sup>2</sup>, 37°C (2:30 PM)**



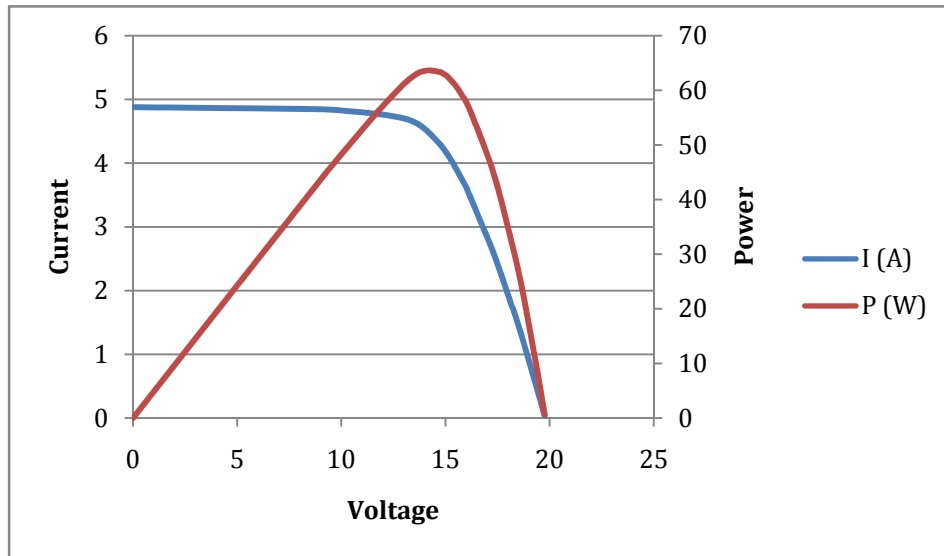
**BP275 Module at 700 W/m<sup>2</sup>, 30°C (3:30 PM)**



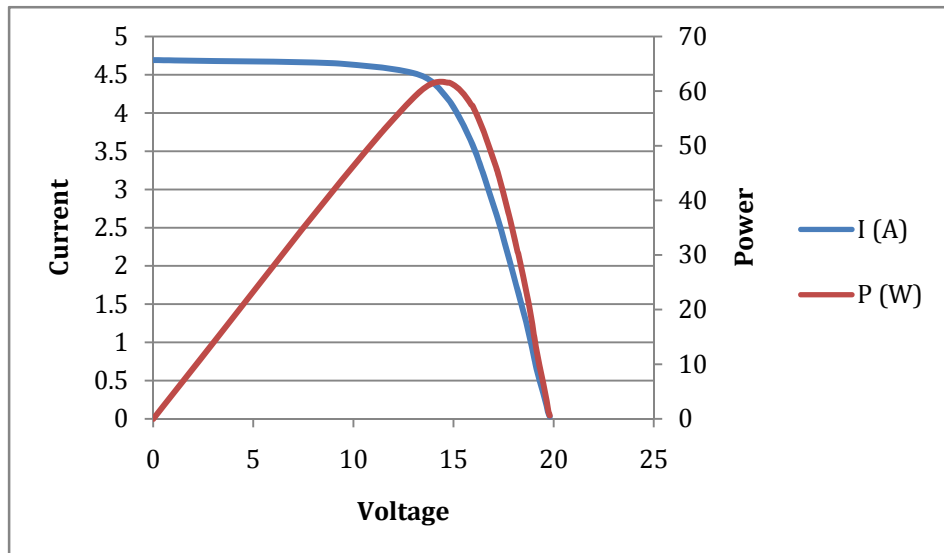
**BP585 Module at 970 W/m<sup>2</sup>, 31°C (10:30 AM)**



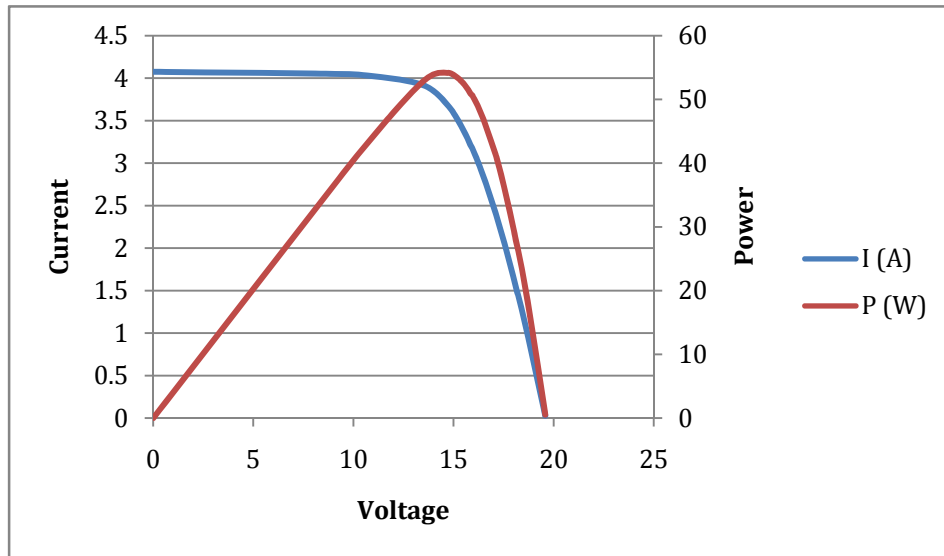
**BP585 Module at 1043 W/m<sup>2</sup>, 30°C (11:30 AM)**



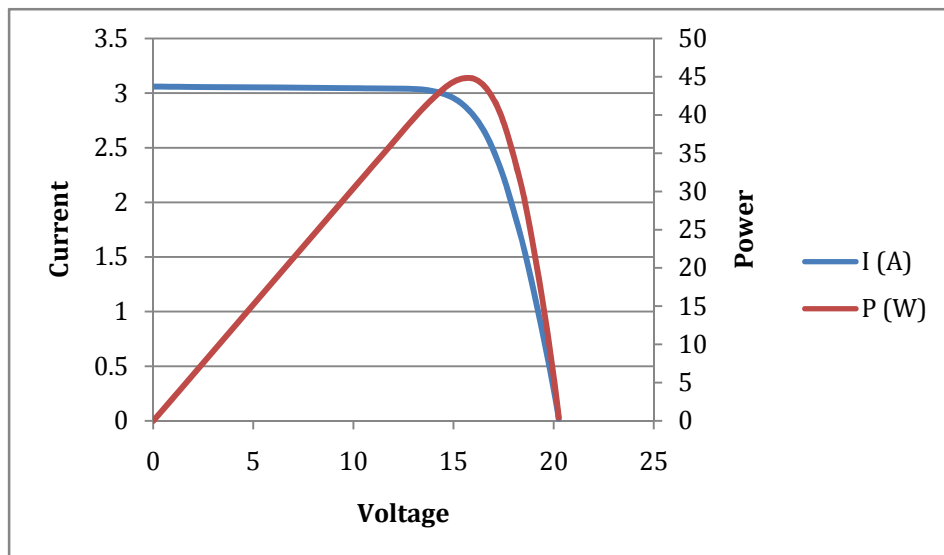
**BP585 Module at 1060 W/m<sup>2</sup>, 32°C (12:30 PM)**



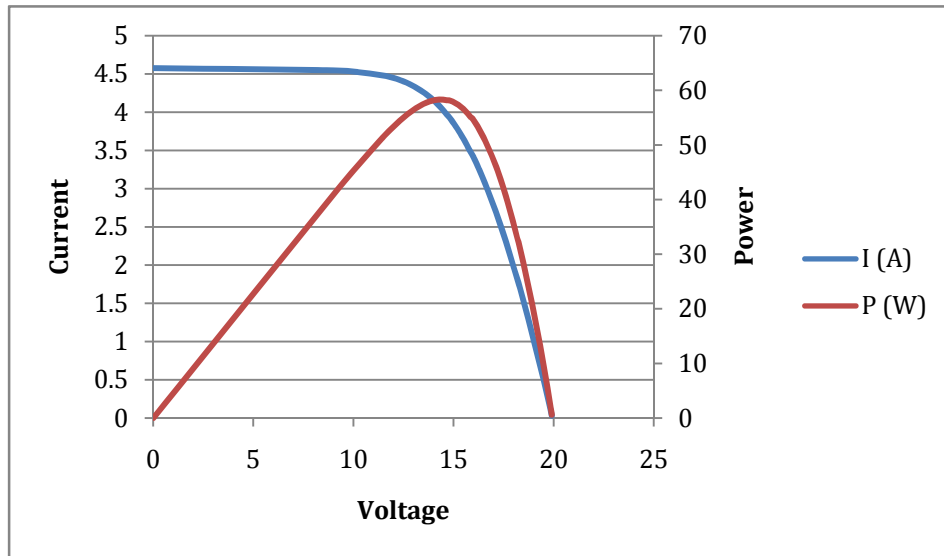
**BP585 Module at 1050 W/m<sup>2</sup>, 33°C (1:30 PM)**



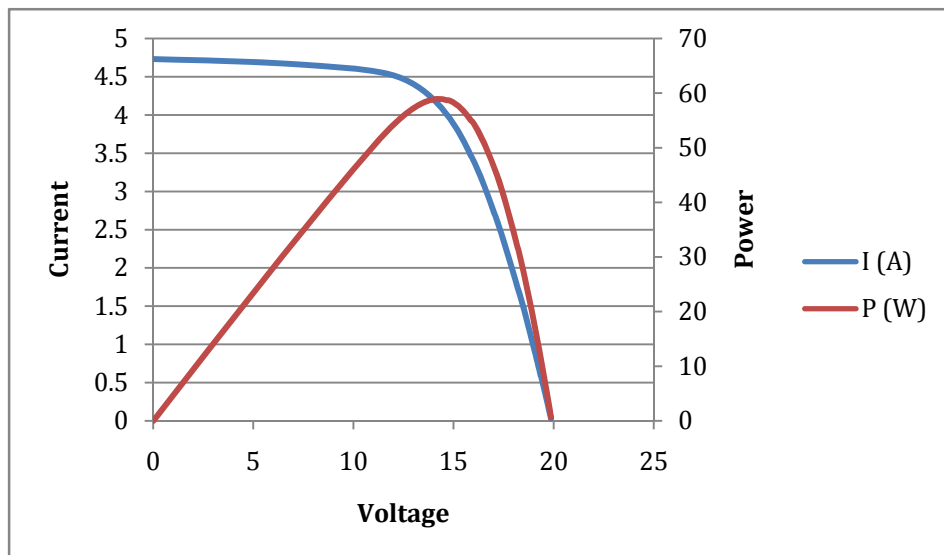
**BP585 Module at 920 W/m<sup>2</sup>, 40°C (2:30 PM)**



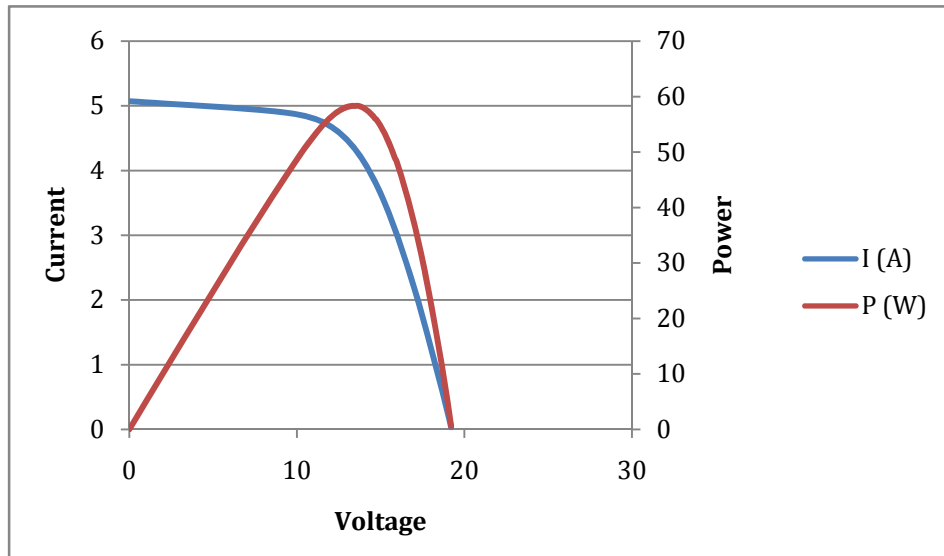
**BP585 Module at 700 W/m<sup>2</sup>, 33°C (1:30 PM)**



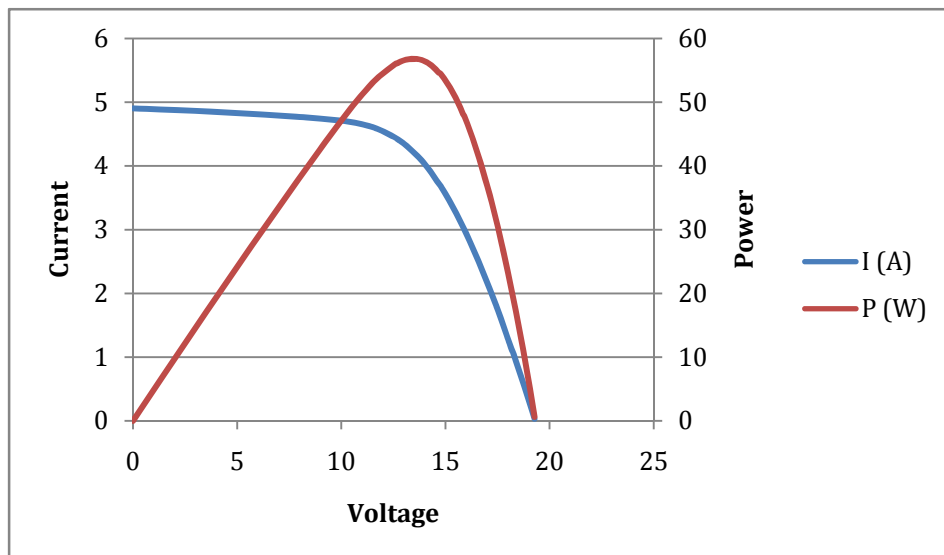
**SX-75 Module at 970 W/m<sup>2</sup>, 31°C (10:30 AM)**



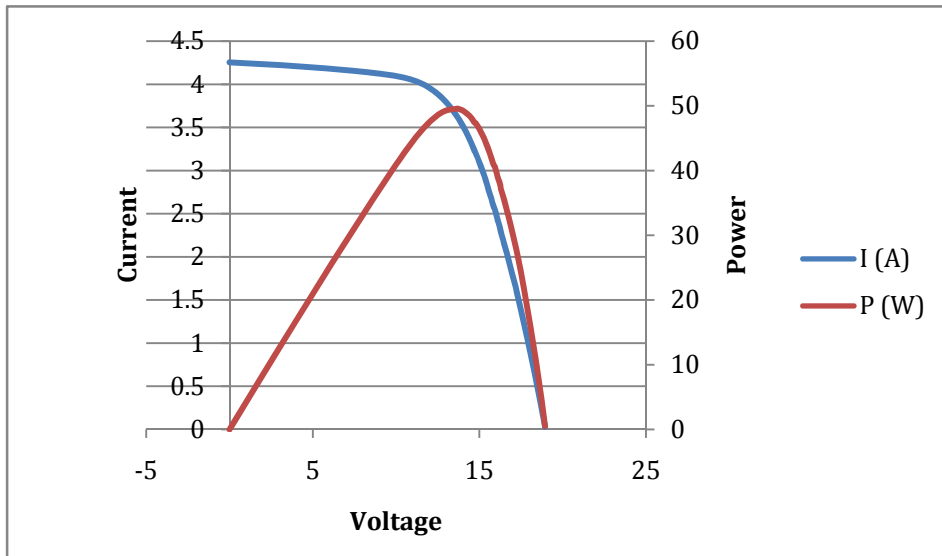
**SX-75 Module at 1043 W/m<sup>2</sup>, 30°C (11:30 AM)**



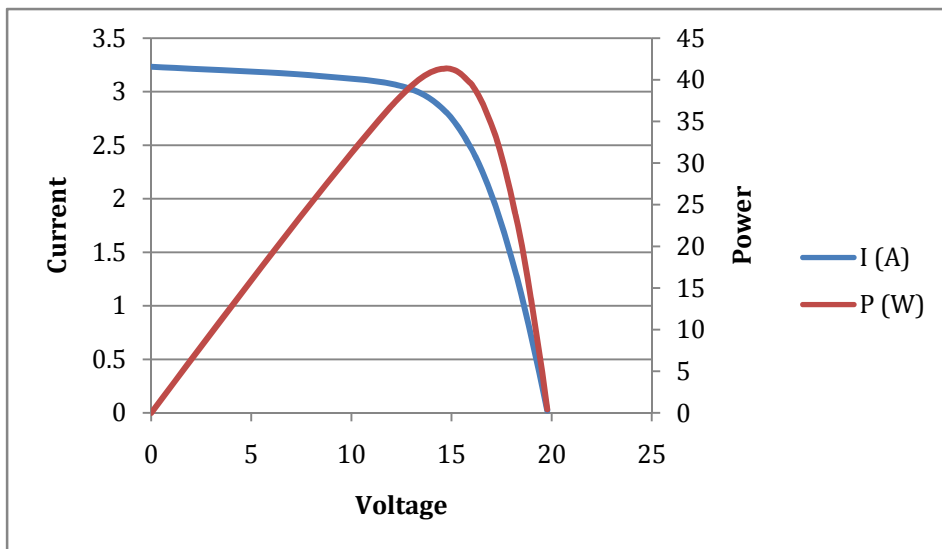
**SX-75 Module at 1060 W/m<sup>2</sup>, 35°C (12:30 PM)**



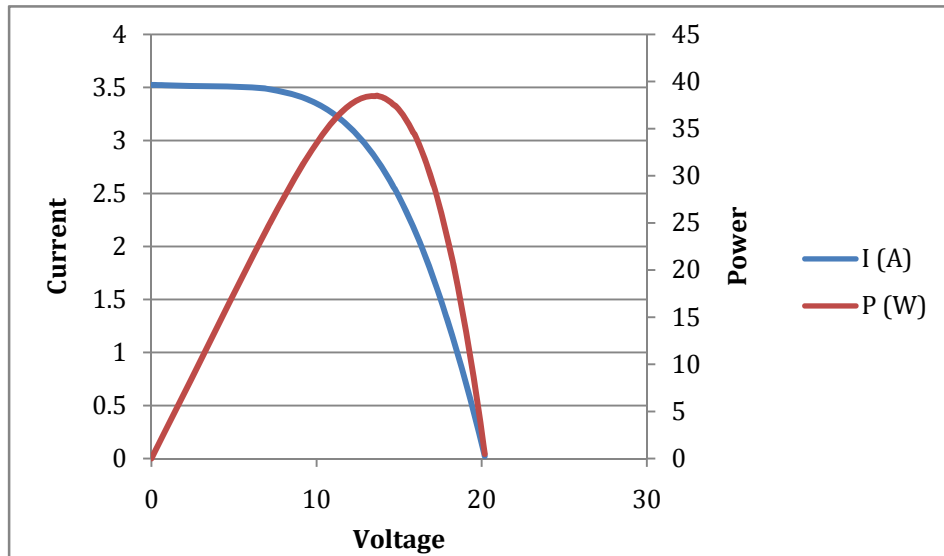
**SX-75 Module at 1050 W/m<sup>2</sup>, 35°C (1:30 PM)**



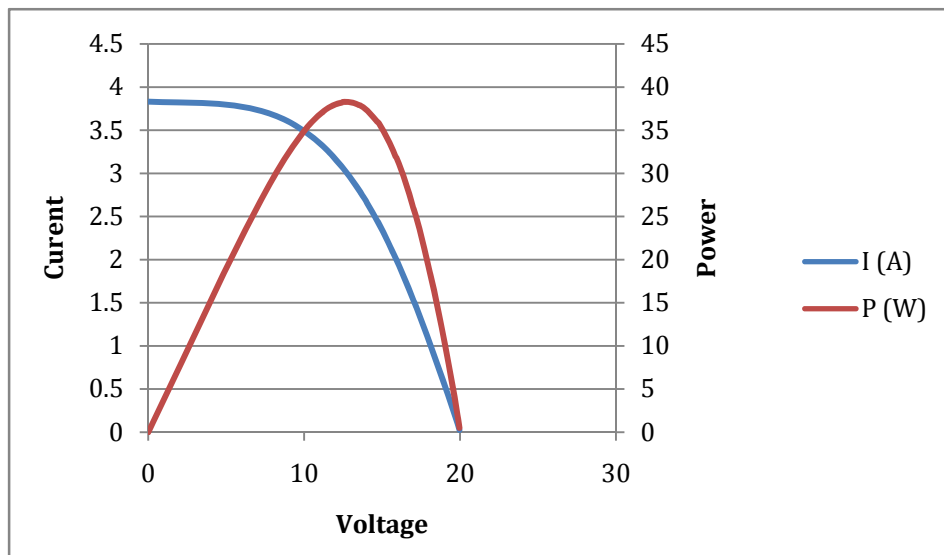
**SX-75 Module at 920 W/m<sup>2</sup>, 40°C (2:30 PM)**



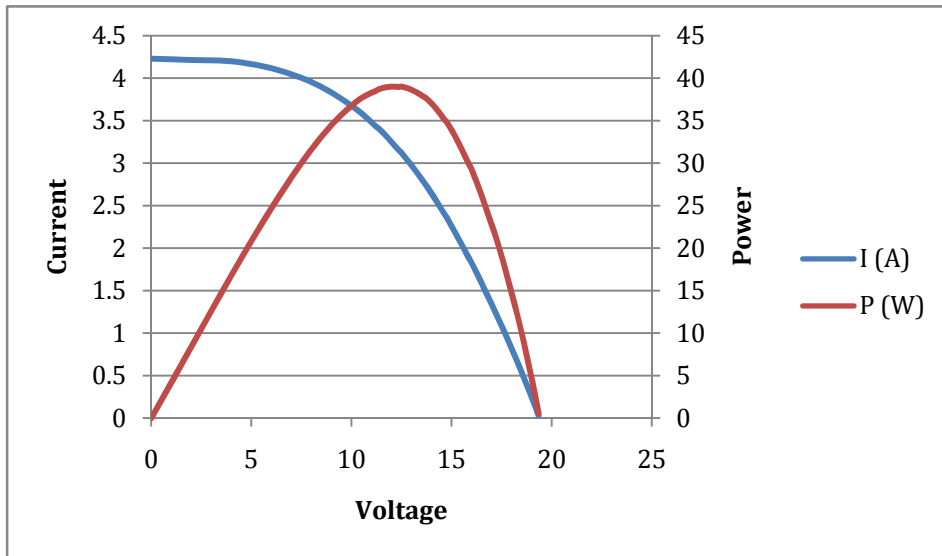
**SX-75 Module at 700 W/m<sup>2</sup>, 27°C (3:30 PM)**



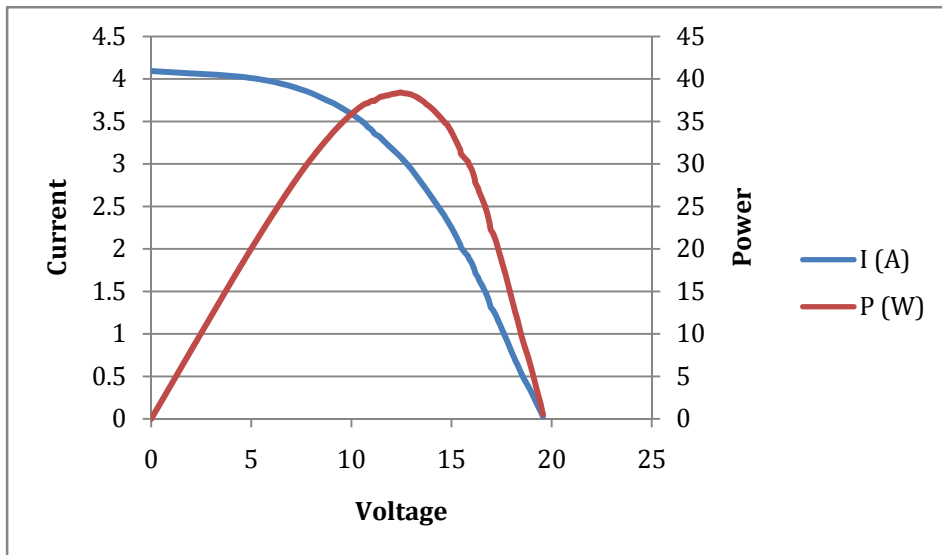
**PW750/70 Module at 970 W/m<sup>2</sup>, 32°C (10:30 AM)**



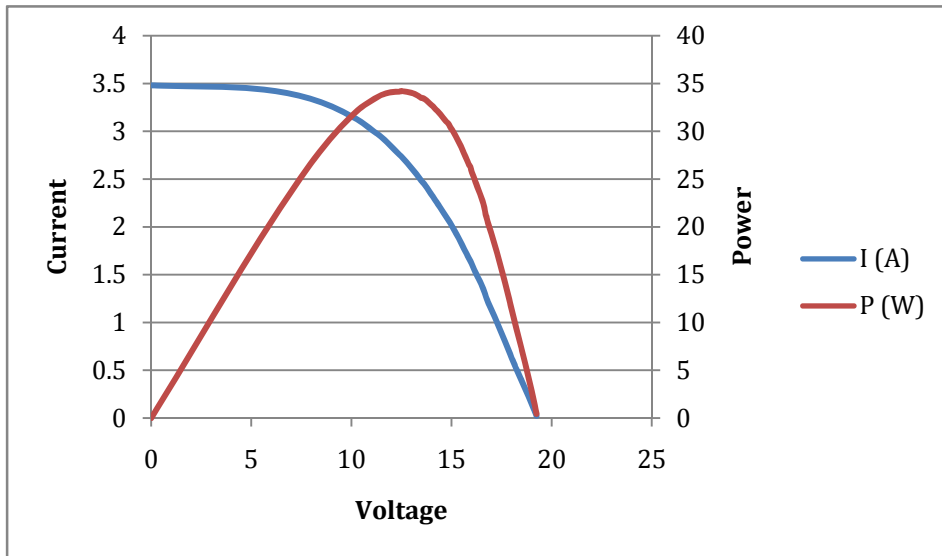
**PW750/70 Module at 1043 W/m<sup>2</sup>, 32°C (11:30 AM)**



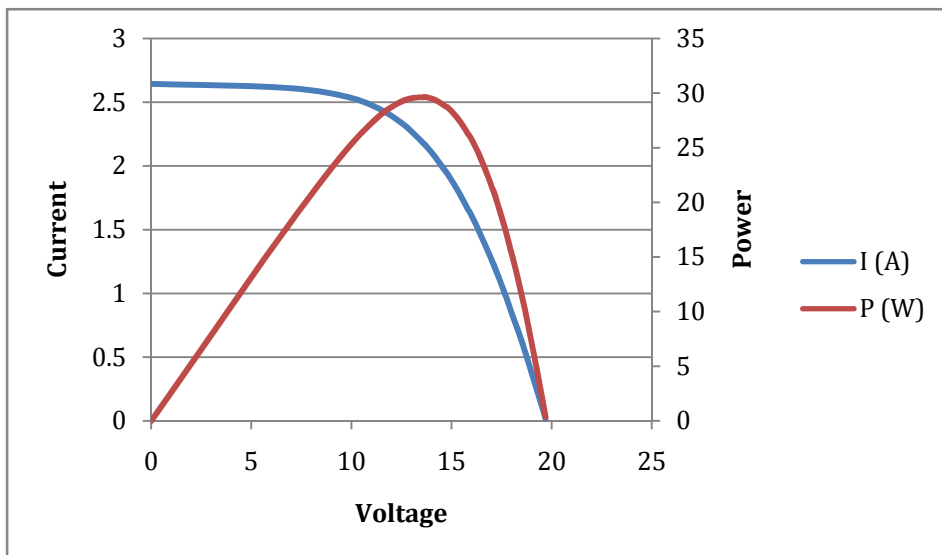
**PW750/70 Module at 1060 W/m<sup>2</sup>, 32°C (12:30 PM)**



**PW750/70 Module at 1050 W/m<sup>2</sup>, 32°C (1:30 PM)**



**PW750/70 Module at 920 W/m<sup>2</sup>, 32°C (2:30 PM)**



**PW750/70 Module at 700 W/m<sup>2</sup>, 32°C (3:30 PM)**